ANNEALING EFFECTS ON PLATINUM COATING MORPHOLOGY

COLANI JOHN MASINA

Thesis presented in fulfillment of the requirements for the degree of Master of Science at the University of Zululand.

Supervisor: Dr. M. Topić

Materials Research Group

iThemba Labs, Cape Town

Co-supervisor: Prof. O.M. Ndwandwe

Dept. of Physics and Engineering

University of Zululand

November 2009

DECLARATION

I, the undersigned, hereby declare that the work contained in this thesis is my own original work except where due reference has been made in the text and that I have not previously in its entirety or in part submitted it at any university for a degree.

Signature: ……

Date: ……

ABSTRACT

The importance of phase transformation for the physical, chemical and mechanical properties of coated systems has been of enormous scientific interest for a long time. Due to a huge application field, the metallic coatings and platinum coated systems in particular, has been studied extensively. Metallic platinum is important for many industrial applications and the demand has increased considerably in the past decade, particularly in applications such as jewellery and catalytic converters (which together account for over 80 % of platinum consumption). In addition, the applications of platinum and its alloys in fuel cells, gas sensors and MEMS are also in increased demand in the last decade. On the other hand, aluminium also plays an important role in electronics, microelectronics and many others applications.

It is known that platinum and platinum alloys readily form intermetallics. Intermetallic compounds based on platinum group metals have almost unique properties. Many of them exhibit outstanding thermodynamic stability in aqueous and elevated temperature applications. Therefore, the platinum group metals base intemetallics are of particular interest as next generation high temperature materials due to their high melting temperatures and better oxidation or corrosive resistance than refractory metals. High melting temperatures of these compounds make them promising candidates for high-temperature structural materials. However, they are hard and brittle which could be a significant limitation when the surface hardness and structural integrity are of importance.

Besides the applications as protective coatings and electronics, the intermetallic phases of the Pt-Al binary system can play a significant role in jewellery industry

where they can contribute towards increased surface hardness without compromising the purity of platinum.

However, the research on platinum/aluminium coated systems conducted in this study was concentrated onto morphological issues and thus, the effect of coating thickness, the temperature and annealing time on coating morphology was studied. Thin platinum coatings deposited on thick aluminium substrates by electron beam deposition process were used as a model system to study the effect of annealing on Pt coating morphology. Samples were annealed in a vacuum furnace at different temperatures and time. Several complementary techniques such as a scanning electron microscope (SEM) equipped with an energy dispersive spectroscopy (EDS), Atomic force microscope (AFM), X-ray diffraction (XRD), Rutherford backscattering spectroscopy (RBS), and Particle induced X-ray emission (PIXE) were used to characterise the coated systems in terms of surface morphology, identification of intermetallics and elemental distribution.

The scanning electron microscope studies revealed that the morphology of thin platinum coatings is affected by both annealing parameters, the temperature and time. Our study showed that rumpling and increased surface roughness, flaking and thickening are the main degradation mechanisms in annealed coated systems. The investigation of phase formation by XRD and RBS revealed the formation of the following intermetallic phases: Al_2Pt, Al_6Pt, $Al_{21}Pt_8$, and $Al_{21}Pt_6$ when annealed at different temperatures and times.

The change in coating morphology has been attributed to the formation of the platinum/aluminium intermetallic phases.

ACKNOWLEDGEMENTS

I would like to extend my gratitude and sincere appreciation to the following group of people, without whose assistance and encouragement this work would not have been possible.

- Dr. M. Topic, Materials Research Scientist, iThemba Labs, for her guidance and encouragement throughout her supervision of this work.

- Prof. O.M. Ndwandwe, Head of Physics Department, Zululand University, for his advises (academic) and input in this work.

- Dr. R. Bucher, Materials Research Scientist, iThemba Labs, for his assistance in analysing X-ray diffraction results.

- Dr. M. Nkosi, Materials Research Scientist, iThemba Labs, he was always there when I needed the e-beam evaporator and annealing furnace.

- Dr. C.Pineda, Materials Research Scientist, expertise in Particle Induced X-ray Emission.

- Mr. P. Sechogela, PhD fellow and Materials Researcher, iThemba Labs, for sharing with me his knowledge of Rutherford Backscattering Spectroscopy.

- My mother, father, and brothers for their support and understanding throughout the time of this work.

- All my friends in and out of the academic field for their support and help.

- National Research Foundation (NRF) for financial support.

- iThemba Labs for facilities and fruitful discussions I had with staff members.

CONTENTS

CHAPTER 1 **BACKGROUND** 1

1.1 Introduction 1

1.2 Importance of Pt and the Pt-Al system 2

1.3 Scope of the investigation 3

CHAPTER 2 **LITERATURE REVIEW** 5

2.1 Theory of phase formation 5

2.2 Theory of diffusion 8

2.3 Models for predicting phase formation in thin film binary systems 11

2.4 Phase formation prediction in Al-Pt thin film system 16

2.4.1 First phase formation 16

2.4.2 Phase formation sequence 19

CHAPTER 3 **SAMPLE PREPARATION AND ANALYSIS TECHNIQUES** 21

3.1 Experimental methods 21

3.1.1 Sample preparations 21

3.1.2 Vacuum annealing 24

3.2 Characterization Techniques 26

3.2.1 Atomic Force Microscopy (AFM) 26

3.2.2 Scanning Electron Microscopy (SEM) 28

3.2.3 X-ray Diffraction (XRD) 31

3.2.4 Particle Induced X-ray Emission (PIXE) 34

3.2.5 Rutherford Backscattering Spectrometry (RBS) 37

CHAPTER 4 **RESULTS** 42

4.1 Surface morphology characterization 42

4.1.1 Atomic Force Microscopy 42

4.1.2 Scanning Electron Microscopy 44

4.1.3 Elemental composition study by PIXE 60

4.2 Phase analysis by XRD and RBS 64

CHAPTER 5 **DISCUSSION** 73

CHAPTER 6 **SUMMARY AND CONCLUSIONS** 79

REFERENCES 83

LIST OF FIGURES

FIGURE 2.1	Gibb's free energy diagram of a growing nucleus of a new phase	6
FIGURE 2.2	Schematic showing the growth of phases in thin film system	7
FIGURE 2.3	Diagram showing an energy barrier of atom	9
FIGURE 2.4	Schematic Showing diffusion mechanisms in solids	10
FIGURE 2.5	Diagram showing an atom occupying an interstitial site	11
FIGURE 2.6	EHF diagram and phase diagram of Pt-Al system	16
FIGURE 3.1	Struers Rotopol-22 polishing machine	22
FIGURE 3.2	High vacuum evaporation system	23
FIGURE 3.3	An Elite thermal systems limited furnace	25
FIGURE 3.4	Atomic force microscopy diagram	27
FIGURE 3.5	Diagram showing heights and depths profiles of a sample	28
FIGURE 3.6	Schematic diagram showing the basic components of SEM	29
FIGURE 3.7	Diagram showing signals generated during sample and electron beam interaction	30
FIGURE 3.8	Image of a Bruker Advance 8 X-ray diffractometer	32
FIGURE 3.9	A diagram showing specular reflection of two parallel X-rays.	34

FIGURE 3.10 Diagram showing creation of a vacancy in a K shell 35

FIGURE 3.11 Diagram showing the filling of a vacancy in a K shell 36

FIGURE 3.12 Image showing the inside of the experimental chamber 37

FIGURE 3.13 Experimental setup for RBS technique 38

FIGURE 4.1 AFM images for as-deposited coatings 43

FIGURE 4.2 SEM micrographs of the as-deposited 0.1 µm Pt coating 44

FIGURE 4.3 SEM micrographs for sample annealed at 200˚C & 400˚C 45

FIGURE 4.4 Coating morphology of samples annealed at 500˚C & 560˚C 47

FIGURE 4.5 Morphology of 0.3 µm Pt layer annealed at 200˚C & 400˚C 49

FIGURE 4.6 SEM micrographs of samples annealed at 500˚C & 560˚C 50

FIGURE 4.7 Morphology of the 0.1 µm Pt layer sample annealed at 590˚C 52

FIGURE 4.8 Morphology of the 0.3 µm Pt coating annealed at 590˚C 53

FIGURE 4.9 Micrographs of the 1hr and 30 min annealed 0.1 µm Pt coating at 500˚C 54

FIGURE 4.10 Micrograph of 0.3 µm Pt coating annealed at 500°C for 30 min 55

FIGURE 4.11 Morphology of 0.3 µm Pt coating annealed at 500°C for 1 hr 55

FIGURE 4.12 Highly magnified micrograph showing nano-size precipitates 57

FIGURE 4.13 Energy dispersive X-ray spectroscopy spectrum 58

FIGURE 4.14 Elemental maps for 0.1 µm Pt layer annealed at 300˚C 61

FIGURE 4.15 PIXE maps for 0.1 µm Pt layer annealed at 590˚C 62

FIGURE 4.16 Elemental mapping of the 0.3 µm Pt layer annealed at 590˚C 63

FIGURE 4.17 XRD patterns for 0.1 µm Pt layer annealed from 300-560˚C 65

FIGURE 4.18 RBS spectra of the 0.1 µm Pt coatings annealed for 30 min 67

FIGURE 4.19 XRD results of the 0.1 µm Pt coatings annealed for 1hr 68

FIGURE 4.20 XRD spectra of the 0.3 µm Pt coatings annealed for 30 min 69

FIGURE 4.21 RBS results for the 0.3 µm Pt layer annealed for 30 min 70

FIGURE 4.22 XRD results of the 0.3 µm Pt coatings annealed for 1hr 72

LIST OF TABLES

TABLE 2.1	Crystallographic and thermodynamic data for the Pt-Al system	14
TABLE 4.1	Average surface roughness of as-deposited samples	43
TABLE 4.2	Coating surface elemental composition analysis	59
TABLE 5.1	Observed intermetallic phases on the 0.1µm Pt coatings	75
TABLE 5.2	Intermetallic phases formed on the 0.3 µm Pt coatings	76
TABLE A	Appendix: Thermal coefficient of common engineering materials	87
TABLE B	Appendix: Melting points of mostly used engineering materials	88

CHAPTER 1 BACKGROUND

1.1 Introduction

The purpose of this research was to study the formation of intermetallic phases in the Al-Pt system. In the time of broader and broader application of thin films and coatings with sophisticated materials structure in the various fields of advanced technologies there is an increasing need to explore the physics and chemistry of the structure forming processes of multicomponent system **[1-2].** The study on mechanism of new intermetallic phase formation by solid state reaction is of considerable interest in the fields of materials sciences **[3-4].** The mechanism of the phase formation as well as the sequence of phase formation is still not fully understood **[1-2].** Classical examples of solid-state reaction are the amorphization and formation of intermetallic phases **[1-2]**. However, the quantitative analysis of kinetics of phase formation is confined essentially to the binary system. This need accelerated the activities in the area of materials science and systematic examination of the phenomena. It is known that phase formation in thin films and coatings requires two steps i.e. (i) migration of the appropriate atoms to suitable locations, (ii) interaction and bonding of the new atoms into the lattice of the newly formed phase **[5].** There has been considerable interest in predicting first phase compound formation and subsequent phase formation sequence during solid state reaction of the elements with each other, but also in the decomposition or phase formation when the phases are in contact with each other. Apart from the obvious academic interest, knowledge of phase formation sequence should enable the materials scientist to control experimental parameters in such a way as to form specific phases with desirable properties.

1.2 Importance of Pt and the Pt-Al system

Particular interest of this study is placed onto aluminium-platinum system. It is known that platinum and platinum alloys readily form intermetallics during heat treatments. Intermetallic compounds based on platinum group metals have unique properties and therefore, are of significant commercial interest **[6, 7]**.

Platinum and aluminium are both used as conductors and interconnects because of their good electrical conductivity and excellent resistance to corrosion **[7, 8]**. The low cost and light weight of aluminium has given the material more attention in metal industry. Such material with light weight finds applications in aircrafts where weight is of great concern. Platinum on the other hand has find many industrial applications, in electrochemical industry where it is used to fabricate electrochemical biosensors **[8].** Platinum and its alloys are thermally stable and are also suitable materials for high temperature applications such as in gas turbine engines **[8, 9].** In catalytic systems Pt is used as a catalyst for the decomposition of hydrogen peroxide into water and oxygen but its performance can quickly degrade through the creation of unwanted by-products, such as hydroxide ions. Hydroxides have an affinity for binding with platinum atoms and when they do this they take those platinum atoms out of the catalytic game. As this platinum-binding continues, the catalytic ability of the cathode erodes. Researchers have been investigating the use of platinum alloys in combination with a surface enrichment technique **[8, 9]**. The Al-Pt coated systems find a broad application in the electronics industry (in integrated circuits as contacts or interconnects), and in the aeroplane industry (inside gas turbine engine to sacrifice for oxidation and corrosion), and in catalytic converters. Pt-Al coated systems also find broader applications in the jewellery and plating industry **[10].**

The phase diagram of the Al-Pt system is very complicated with many equilibrium phases **[6, 10, 11]**. However, despite the extensive work on these materials, the principles underlying the formation of various phases are still not fully understood. Therefore, the main aim of this research was to study the effects of annealing parameters such as temperature and time on the thermodynamics and kinetics of intermetallics formation and their effects on coating morphology. To study the effects of annealing on the morphology of Pt coatings Al was chosen as a substrate material. Al was preferred because it readily forms intermetallic phases with Pt and the formation of these intermetallics can induce morphological developments on the coatings. Another benefit of using Al was that it improves the surface hardness of Pt without compromising its purity **[10]**. Economically it was also an advantage to use Al because of its low cost but not underestimate its good properties.

1.3 Scope of the investigation

Thin Pt coatings deposited on thick Al substrates were studied and particular interest of this research has been placed on phase formation and subsequent effect on coating morphology. Different models used to predict first phase formation and phase formation sequence in the metal-metal systems and Pt-Al binary system in particular are discussed. The materials, experimental techniques and methods used for this investigation are described in chapter 3. Chapter 4 gives experimental results of the phase formation in the Al-Pt coated system. The surface morphology of the Pt coatings with thickness of 0.1 µm and 0.3 µm at temperatures ranging from 200-600 °C were studied by scanning electron microscopy and atomic force microscopy analysis. The experimental results also include the investigation of the solid state

interaction and elemental distribution of Al and Pt using nuclear microprobes techniques such as Rutherford backscattering spectroscopy (RBS) and elemental distribution analysis. The discussion and conclusions drawn from this study are presented in chapter 5 and chapter 6 respectively.

CHAPTER 2 LITERATURE REVIEW

2.1 Theory of phase formation

Theory of phase formation is very important in thin films and coatings because it enables materials scientist to predict which phase will start to nucleate in a particular system and also phase formation sequence can be achieved by using this theory **[1, 2, 11,13]**. There are two models which were very successful in predicting first phase formation and they are still in use today: (i) the model proposed by Walser and Bene (ii) and the effective heat of formation (EHF) model **[11, 13].** These two models are the only models which make good prediction regarding first phase formation. The formation of a new compound involves migration of atoms between the two solids and subsequently consists of formation and growth of nucleus. The kinetics of phase formation of thin films has been reported in the literature **[14]**. Two types of growth kinetics have been discovered in thin films, which are diffusion controlled kinetics and reaction controlled reaction.

It is of great importance to understand growth kinetics in thin films, because the manner in which the thickness of a phase grows with time is recognized through the knowledge of growth kinetics. Considering the solid-state reaction there is two types of systems: (a) the systems that show lateral non-uniform growth which is temperature dependent (the kinetics of growth is difficult to establish in these systems); and (b) the system that show laterally uniform growth with well defined kinetics and temperature dependence and therefore, it is easy to establish some form of growth **[15]**. Atoms of both elements A and B must come together at the interface

or reaction zone to form a nucleus of appropriate composition and structure for the formation of a compound $A_\alpha B$ between the two solids as shown in fig. 2.2. In order to grow, the newly formed nucleus must have a radius greater than the critical radius r*, as shown in figure 2.1. The formation of a nucleus means the formation of a new surface and it is associated with the increase in surface energy. A new phase can only be formed when there is reduction in the Gibb's free energy ΔG of the system. If the surface energy is increasing it also increases the Gibb's free energy and phase formation is not expected to occur (in this case surface energy acts as a barrier for the nucleation of a new phase).

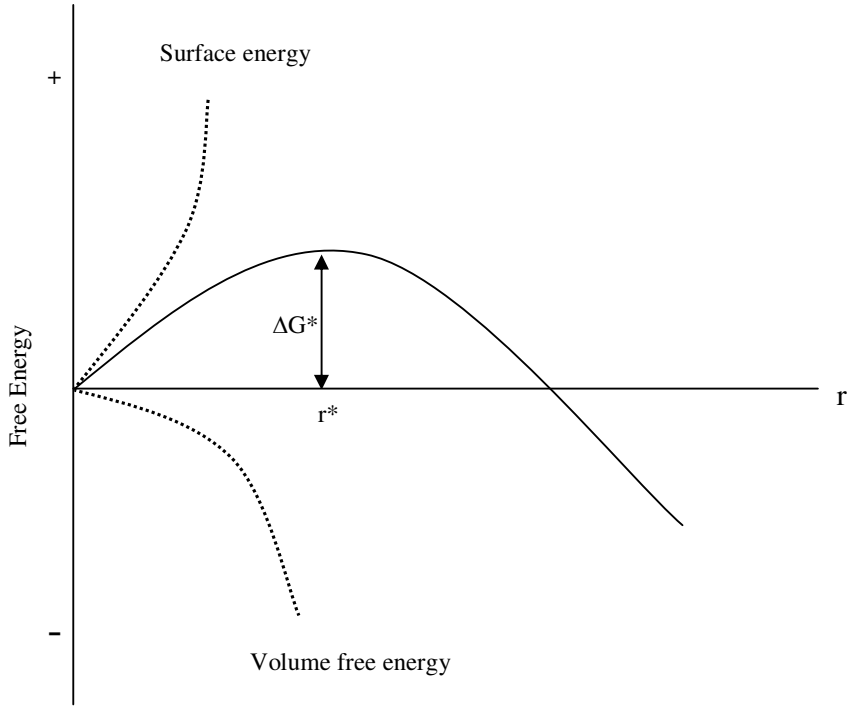

Figure 2.1: The activation energy barrier ΔG* and the critical radius size r* of a growing nucleus. Three curves are showing the contribution of the surface energy, volume energy and their sum ΔG (Gibbs free energy) [16].

The Gibb's free energy as a function of nuclei radius, surface and volume energy at a given temperature is given by **[16]**:

$$\Delta G = \frac{4}{3}\pi r^3 \Delta G_v + 4\pi r^2 \Delta\sigma \qquad (2.1)$$

where ΔG_v is the Gibb's free energy per unit volume and $\Delta\sigma$ is the surface energy per unit area.

The sum of the first and second term in equation 2.1 is decreasing as the radius of the formed nucleus is increasing and this reduces the Gibb's free energy even though the surface energy is increasing. Under this condition the formation of a nucleus is favoured. After nucleation the next process is growth. The compound growth process may be proportional to either time or to the square root of time depending on the limiting mechanism responsible for the compound growth. Let us take that element A is the diffusing species in this particular binary system (see fig.2.2).

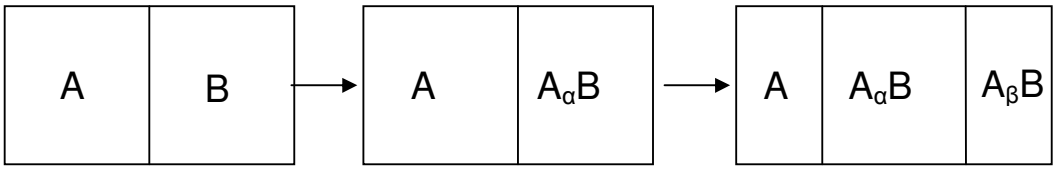

Figure 2.2: Schematic showing the growth of different phases in a binary thin film system.

Atoms of element A must diffuse through the growing $A_\alpha B$ phase in order to reach the area of reaction i.e. reaction zone. This is relatively easy at the early stages of the reaction because the $A_\alpha B$ phase is very thin for the A atoms to diffuse through, but later during the reaction the $A_\alpha B$ phase becomes thicker and A atoms starts to experience some diffusion barriers. In this case the growth rate of the compound $A_\alpha B$

will start to slow down due to limited transport of materials through the growing compound to the area of reaction (i.e. diffusion of A atoms through the $A_\alpha B$ phase to $A_\alpha B$-B interface where it will get together with B atoms and they react). This growth rate shows a parabolic relationship with time and it is called *diffusion controlled kinetics.* While the other systems show growth rate which shows linear relationship with time and this kind of growth mechanism it termed *reaction controlled kinetics* **[14]**. The silicides can show growth rate which is *nucleation controlled* **[14, 17].** However, the attention will be paid to diffusion controlled kinetics since the Pt-Al system is of particular interest in this study.

2.2 Theory of diffusion

Diffusion is the movement or transport of matter from a region of high concentration to a region of low concentration. Changes in solids (chemical reactions and micro-structural changes) happen because of diffusion **[3]**. Atomic diffusion occurs during heat treatments, materials are heat treated to enhance properties such as mechanical thermally, and structural etc. Atoms in solids vibrate or oscillate around their equilibrium positions in the crystal lattice **[16, 19, 20**]. During heat treatments atoms gain enough energy to break those bonds and change their sites. This gives rise to diffusion a process. Figure 2.3 shows the energy barrier (ΔG) for an atom to move to a vacancy position **[16, 19, 20]**. For diffusion to occur the atom in position A require enough energy (energy to overcome the barrier ΔG) to move to vacancy position B.

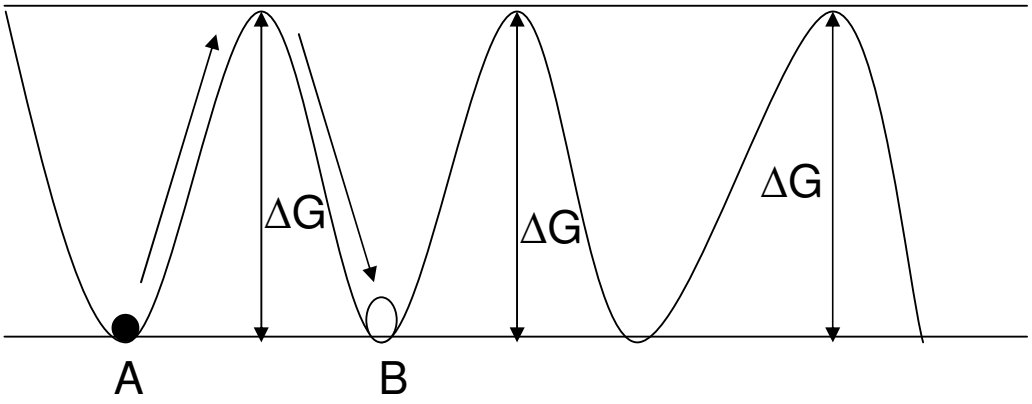

Figure 2.3: Diagram showing an atom in its lattice position A and a vacancy in position B. ΔG is the energy barrier that an atom must overcome to move from position A to a vacancy position B [18].

Diffusion in solids takes place because of the presence of defects **[3]**. Different types of defects give rise to different types of diffusion mechanisms. For diffusion to occur the following conditions must be satisfied:

- **There must be an adjacent empty site.**
- **Atoms must have sufficient energy (activation energy) to break bonds with its neighbors and migrate to adjacent site.**

A solid at any temperature always contains defects (due to entropy) and this satisfies the first condition **[18]**. The second condition can be satisfied by heat treating the material, because during heat treatment atoms get excited and gains more energy. Figure 2.4 shows the different diffusion mechanisms that are common in solids.

1. **Vacancy mechanism**-If an atom on a normal site jumps into an adjacent unoccupied lattice site (vacancy) this type of diffusion is said to be vacancy diffusion (a).

2. **Interstitial mechanism-** This type of diffusion occurs when an atom on an interstitial site moves to one of the neighboring interstitial sites (b).
3. **Interstitialcy mechanism**-In the interstitialcy mechanism an interstitial atom pushes a lattice atom into an interstitial site and itself taking the place of the displaced lattice atom (c). Sometimes diffusion can occur when atoms swap positions (d, e).

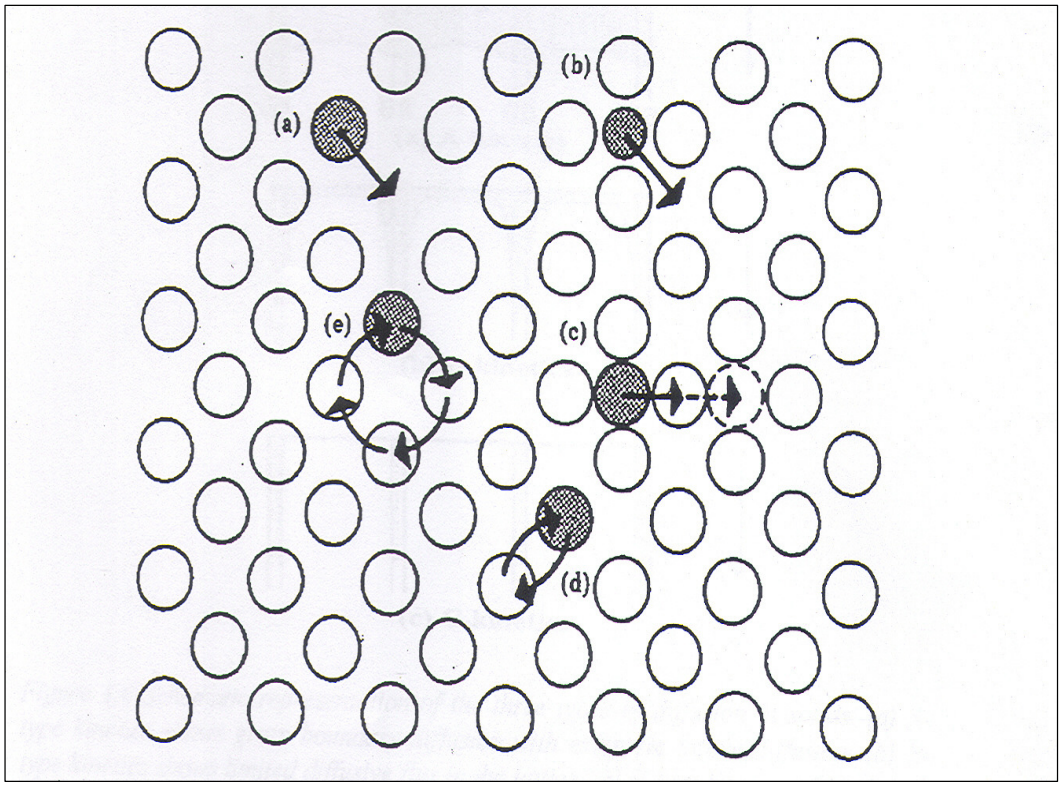

Figure 2.4: Schematic diagram showing five kinds of diffusion mechanisms taking place in solids [16].

Diffusion of atoms can give rise to structural disorder in a lattice. Figure 2.5 shows a disorder that results when a bigger atom occupies an interstitial position or site and it is termed lattice distortion.

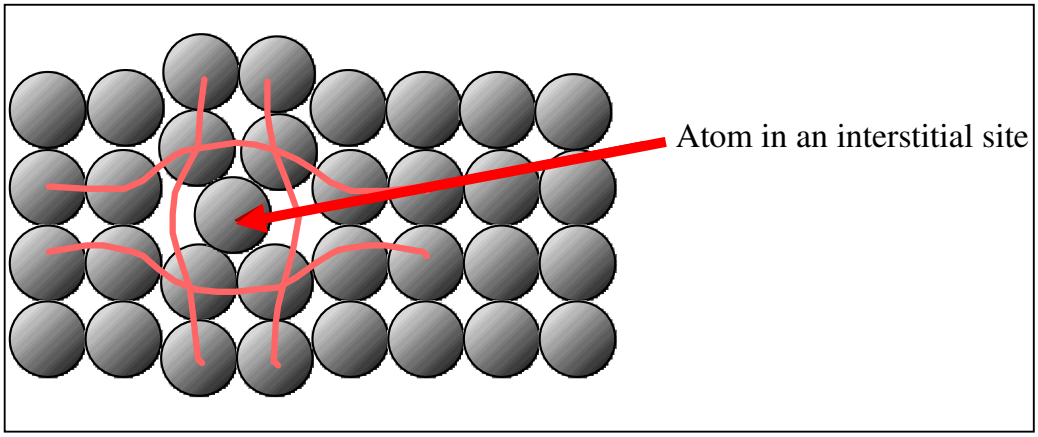

Figure 2.5: Schematic diagram showing an atom occupying interstitial site in a perfectly crystal structure [20].

As a consequence of diffusion, the formation and migration of vacancies is observed during an annealing process which results in change of the crystal structure of the materials **[19, 28, 29]**. The phase transformations, formation of new phases and the sequence of their formation were of particular interest. Many models have been proposed to predict the phase formation in thin film systems. However, many of them were not able to predict the sequence of phase formation correctly.

2.3 Models for predicting phase formation in thin film binary systems

The model proposed by Walser and Bene **[11, 12, 21]** is one of the earliest models used to predict first phase formation and phase formation sequence. Using this model the following rule was formulated for predicting phase formation at metal/silicon planar interface:

"The first compound nucleated in planar binary reaction couples is the most stable congruently melting compound adjacent to the lowest-temperature eutectic on the bulk equilibrium phase diagram".

This rule was later extended to metal-metal systems by relaxing the requirement that the first phase that forms needs to be congruently melted. The extended rule states that:*"The first phase nucleated in metal-metal thin film reactions is the first immediately adjacent to the low-temperature eutectic in the binary phase diagram"*.

There is "phase skipping" in the metal-silicon rule; the non-congruently melting phases are not predicted by this rule, which makes this rule very dissimilar to the rule applied for the metal-metal systems. The metal-metal rule makes no reference to the stability of the phase in the case where the eutectic lies between the two phases. This rule only predicts that it is the phase immediately adjacent to the lowest –temperature eutectic that will form.

Pretorius *et al.* **[4]** proposed the effective heat of formation (EHF) model after Walser and Bene. The EHF model uses thermodynamics properties such as entropy, enthalpy, and Gibb's free energy to predict first phase formation and phase formation sequence **[11, 12, 21]**. This is a reasonable model because it is known that a phase has a set of properties including this mentioned thermodynamics properties. In this model effective heat of formation ($\Delta H'$) is used to predict first phase formation. Effective heat of formation ($\Delta H'$) is calculated as function of effective concentration of the reacting species at the reaction zone or interface. The stability of a system is determined by its Gibb's free energy (ΔG). At constant temperature and pressure the change in Gibb's free energy is given by:

$$\Delta G^0 = \Delta H^0 - T\Delta S^0 \tag{2.2}$$

where ΔH^0 is the change in enthalpy (heat of formation), T is the absolute temperature, and ΔS^0 is the change in entropy of the system. For solid-state reactions the product $T\Delta S^0$ is usually very small (ΔS^0 is in the order of 0.001 *kJ/deg per mole of atoms*), therefore ΔG^0 may be approximated by ΔH^0 i.e. $\Delta G^0 \approx \Delta H^0$ Phase formation at interface is a dynamic non-equilibrium process; in this case equilibrium rules cannot be applied directly. Unlike in equilibrium systems where formation of a mixture of phases might lead to the lowest Gibb's free energy, in non-equilibrium systems usually only one phase grows at a certain interface.

To illustrate the concept of effective heat of formation model (EHF) one must consider an example. Suppose there are two solids in a system, for instance Pt and Al which they interact at a particular interface. The available concentration of both Al and Pt at the growth interface must be considered. This concentration is the effective concentration of the reacting species and it is not the actual concentration of the two solids. There are some factors that can be accountable for this discrepancy (difference between actual concentration and effective concentration). Amongst these factors are diffusion barriers, impurities, atomic mobility, not a clearly defined liquidus minimum, etc. So far, it is still not possible to calculate the actual effective concentration at the growth interface during solid-state reaction. This problem was tried to be solved by using the idea of Brown and Ashby which states that for a given structure and bond type, the activation energy for solid-state diffusion is directly proportional to the melting temperature of the solid. The activation energy determines the mobility, the smaller the activation energy the greater the mobility of atoms. Upon heating it is expected that the utmost mobility of atoms and the most effective mixing at the reaction zone takes place at the composition corresponding to the liquidus

minimum of that particular system. The concentration leading to the highest mobility of atoms is therefore taken as the effective concentration; this concentration is given by the composition at the liquidus minimum of the binary system. Table 2.1 shows the effective crystals concentration of Al and Pt at the growth interface was Arbitrarily taken as 98 at.% Al and 2 at.% Pt.

Table 2.1: Crystallographic and thermodynamic data for equilibrium Pt-Al phases. The effective heats of formation (ΔH`) have been calculated at a concentration of 2 at.% Pt and 98 at.% Al [6].

Phase	crystal system	Lattice constants (nm)	Atoms in unit cell	ΔH^0 kJ(mol.at.)$^{-1}$	ΔH' kJ(mol.at.)$^{-1}$
Pt_3Al	tetrag.	0.5459 0.7806	16	-70	-1.87
Pt_2Al	Orthor.	1.6306 0.3919 0.5433	24	-88	-2.64
Pt_5Al_3	Orthor.	0.541 1.07 0.395	16	-88	-2.82
PtAl	cubic	0.4866	8	-100	-4.00
Pt_2Al_3	hexag.	0.4209 1.035	5	-95	-4.75
$PtAl_2$	cubic	0.591	12	-84	-5.05
Pt_8Al_{21}	tetrag.	1.298 1.065	116	-71	-5.14
Pt_5Al_{21}	cubic		416	-57	-5.94

An example on how to calculate the effective heat of formation for a compound can be made using the formation of Pt_2Al compound. In order to form the Pt_2Al

compound two platinum atoms are needed for every one aluminium atom, the concentration of Al at the growth interface is higher than that of platinum (more aluminium is present compared to platinum), it is therefore expected that the platinum is first used up before the aluminium. This makes platinum to become the limiting element for the formation of Pt_2Al compound and Al atoms will be in excess. It has been mentioned earlier on that phase formation at the growth interface is a dynamic nonequilibrium process and therefore the excess Al atoms will be available for the formation of the next increment of the compound at the moving interface instead of contributing to the heat released by system when forming that particular compound. All the heat released by the system in the formation of a particular compound is determined by the effective concentration of the limiting element; because the excess element does not contribute to heat released by the system instead it initiates the formation of the next compound. The effective heat of formation (ΔH`) as a function of effective concentration is defined as **[21]**:

$$\Delta H' = \Delta H \times \left(\frac{effective\, conc.\lim.element}{compound\, conc.\lim.element} \right) \tag{2.3}$$

In the example mentioned above the effective concentration for the formation of the Pt_2Al becomes

$$\Delta H' = (-88) \times \left(\frac{0.02}{0.667} \right) = -2.64\, kJ\,(mol.at.)^{-1}$$

The effective heat of formation for each compound in a system can be calculated by using equation 2.3. Using this equation it can be possible to predict first phase

formation and formation sequence in binary metal systems. The EHF model was used to predict first phase formation and phase formation sequence in the Al-Pt system.

2.4 Phase formation prediction in Al-Pt thin film system

2.4.1 First phase formation

The Pt-Al system is very complicated with many equilibrium phases **[1]**. Figure 2.6 shows the effective heat of formation diagram as well as phase diagram for Pt-Al system.

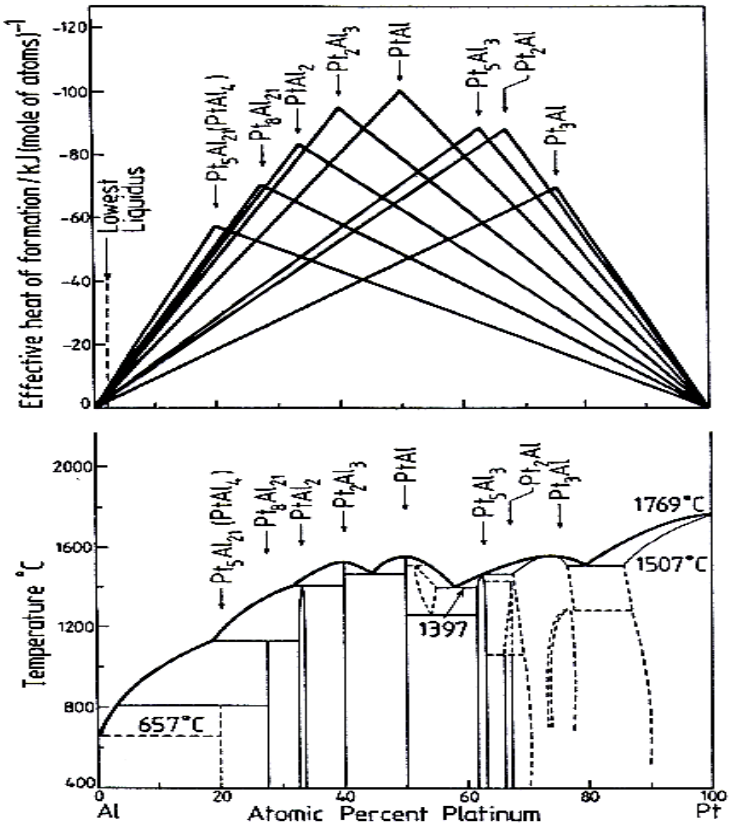

Figure 2.6: The effective heat of formation diagram for compound phase formation (top) and the phase diagram (bottom) for the Pt-Al system [6].

Pretorius *et al.* **[21]** reported that the EHF model could be successfully used to predict first phase formation and phase formation sequence in aluminides. However, the effective concentration of the two reacting species at the growth interface must be known in order to predict first phase formation using this model. In section 2.3 it has been explained that the effective concentration of the reacting elements in solid-state reaction is the concentration of these species at the composition of the liquidus minimum. It is found that the liquidus minimum is at the melting point of Al in the case of aluminides. An effective concentration of 98 at.% Al and 2 at.% metal was in that case arbitrarily chosen **[21]**. It must be remembered that for a phase to be formed there must be a change in the free energy of the system. Phases with most negative effective heat of formation ($\Delta H'$) are expected to lead to the largest change in free energy. It does not always mean that a phase with the most negative EHF value will be the first to form as nucleation barriers can prevent its formation. Pretorius *et al.* **[12]** identified some factors that can prevent a phase from nucleating at the interface:

- **Number of atoms per unit cell**- phases with large number of atoms per unit cell finds it difficult to nucleate.
- **Temperature** – nucleation is favored by high temperatures, because there is high mobility of atoms at high temperatures.
- **Crystal structure** - complex crystal structures are not expected to nucleate more readily compared to simple crystal structures.
- **Directionality of bonding** - nucleation tend to be more difficult for bonding which is highly directional than metal-metal bonding which is non-directional.

From the thermodynamic data in Table 2.1 it can be seen that the phase Pt_5Al_{21} has the most negative effective heat of formation value [$\Delta H'$ = -5.94 kJ (mol.at.)$^{-1}$]. The formation of this phase is expected to lead to the largest change in free energy, but most thin film studies showed that Pt_2Al_3 is the first phase to form. The principal difference between the two phases is the number of atoms per unit cell, there are 416 atoms per unit cell in the Pt_5Al_{21} and 16 atoms per unit cell in the Pt_2Al_3 phase. Because the number of atoms per unit cell is one of the factors that can affect nucleation, it is not surprising that Pt_2Al_3 is observed to form first instead of Pt_5Al_{21}. Another phase with the most negative heat of formation following Pt_5Al_{21} phase is Pt_8Al_{21} with 116 atoms per unit cell, again the formation of this phase can lead to the largest change in free energy but nucleation barriers prevents its formation. However it is very difficult to take into considerations the nucleation barriers in interactions in thin films, because the EHF model alone which does not take nucleation into account predicts certain phases to form first but experimentally it's not confirmed. When nucleation is taken into consideration, the EHF model would predict first phase formation of $PtAl_2$ or Pt_2Al_3. It is not very clear which phase forms first between the two phases. Their $\Delta H'$ values are very close, -5.05 kJ (mol.at.) for $PtAl_2$ and -4.75 kJ (mol.at) for Pt_2Al_3. The $PtAl_2$ phase has 12 atoms per unit cell compared to Pt_2Al_3 with 5 atoms per unit cell. In most thin films studied so far Pt_2Al_3 is found to be the first phase to form, which is a congruent phase with less number of atoms per unit cell. The difficulty in opting the exact phase comes from the fact that thermodynamic quantities are seldom known with accuracies of better than 10% **[4, 12, 21]**. The EHF rule for first formation when nucleation barriers are not taken into account thus states that: *"The first-compound phase to form during metal-metal interaction is the phase*

with the most negative, effective heat of formation ($\Delta H'$) at the concentration of the lowest temperature eutectic (liquidus minimum) of the binary system".

2.4.2 Phase formation sequence

In thin-films and coating systems under steady state annealing conditions usually only one of the equilibrium phases grow at a time **[4, 6, 17, 23]**. This phase will then grow until one of the reactants at the reaction zone is completely consumed. The elements A and B are present at the start of the reaction, these two elements react to form compound phase $A_\alpha B$ and this phase will grow until one of the two elements is completely consumed (element B in this case). The reaction between the remaining element A and the formed phase $A_\alpha B$ will result in the formation of a new phase $A_\beta B$. The $A_\beta B$ phase will grow until either $A_\alpha B$ or element A is completely consumed. The effective heat of formation rule for phase formation sequence in metal-metal systems states that:

"After first-phase formation in metal-metal binary systems, the next phase to form at the interface between the compound phase and remaining element is the next phase richer in the unreacted element, which has the most negative effective heat of formation".

As it has been mentioned earlier that focus of this work is on the Al-Pt coated system. Let us now explore this system as far as the phase formation is concerned. The effective heat of formation rule for first phase formation predicts that Pt_2Al_3 is the first phase to form in Al-Pt system since its formation will lead to the biggest change in Gibb's energy (section 2.4.1). According to the demonstration shown earlier in fig. 2.2 the Pt_2Al_3 phase will grow until the entire Pt or the entire Al is consumed. The availability of the two elements (Pt and Al) will determine whether the next phase to form after the Pt_2Al_3 phase will be Al-rich or Pt-rich. In the case of thin Pt on top of

thick Al (Al>Pt) more Al is available than Pt, this means that the entire Pt will be consumed. The consumption of Pt during the reaction reduces its effective concentration; therefore the relative concentrations of the reactants will move to the left-hand direction of figure 2.6. The phase with the most negative heat of formation on the left-hand side of Pt_2Al_3 is likely to form, $PtAl_2$ is the one with the most negative EHF value and its formation will lead to the biggest change in free energy. If there is still Al present after the transformation of Pt_2Al_3 to the $PtAl_2$ the effective concentration of the atoms will move further to the Al-rich region where the formation of $PtAl_4$ is expected. The formation of Pt_8Al_{21} and Pt_5Al_{21} can lead to the biggest change in free energy, but their difficulty in nucleating prevents their formation. Let us now consider the case of thick Pt on top of thin Al (Pt>Al), Pt_2Al_3 is again expected to form first. All the aluminium will be consumed before platinum and this decreases the effective concentration of Al. if the effective concentration of Al decreases then the relative concentration moves to the right of the effective heat of formation (fig. 2.6). The remaining Pt will initiate the transformation of Pt_2Al_3 to PtAl. The PtAl phase will be followed by the formation of Pt_5Al_3, Pt_2Al, and Pt_3Al phases. The further formation of intermetallic phases is possible only if there is still unreacted Pt or Al remaining in the system to initiate the transformation.

The phase transformations in coated systems in general, have been of significant scientific and practical interest. It is due to the fact that the knowledge of phase formation sequence enables scientists to form specific phase or combination of different phases according to the particular needs. Thus, the coated systems could be designed in such a way to have desirable properties depending on particular service requirements.

CHAPTER 3 SAMPLE PREPARATION AND ANALYSIS TECHNIQUES

3.1 Experimental methods

In this work, the electron beam evaporation system was used to deposit thin platinum films on thick aluminium substrates. The deposited coatings were annealed and their morphology and phase formation were investigated. This chapter is separated in to two major sections; section 3.1 describes the subject of the preparation of platinum thin film coatings on aluminium substrates and section 3.2 focus on the analytical techniques used to analyze the coating systems used in this study.

3.1.1 Sample preparations

Aluminium (99.999 wt. % purity) as a substrate and pure platinum (99.99 wt. %) as coating materials were used in this study. Aluminium plate of 100×100 mm was cut into 10 mm x 10 mm squares. The thickness of the Al substrates was approximately 1.5 mm. The Al substrates were mechanically polished using the Struers automatic polishing machine (fig. 3.1). Polishing was accomplished by bringing the Al substrates into contact with the polishing cloth (pad) which had diamond polishing slurry on top of it. The contact between the samples and the polishing cloth was made possible by the motorized rotating wheel or sample mover.

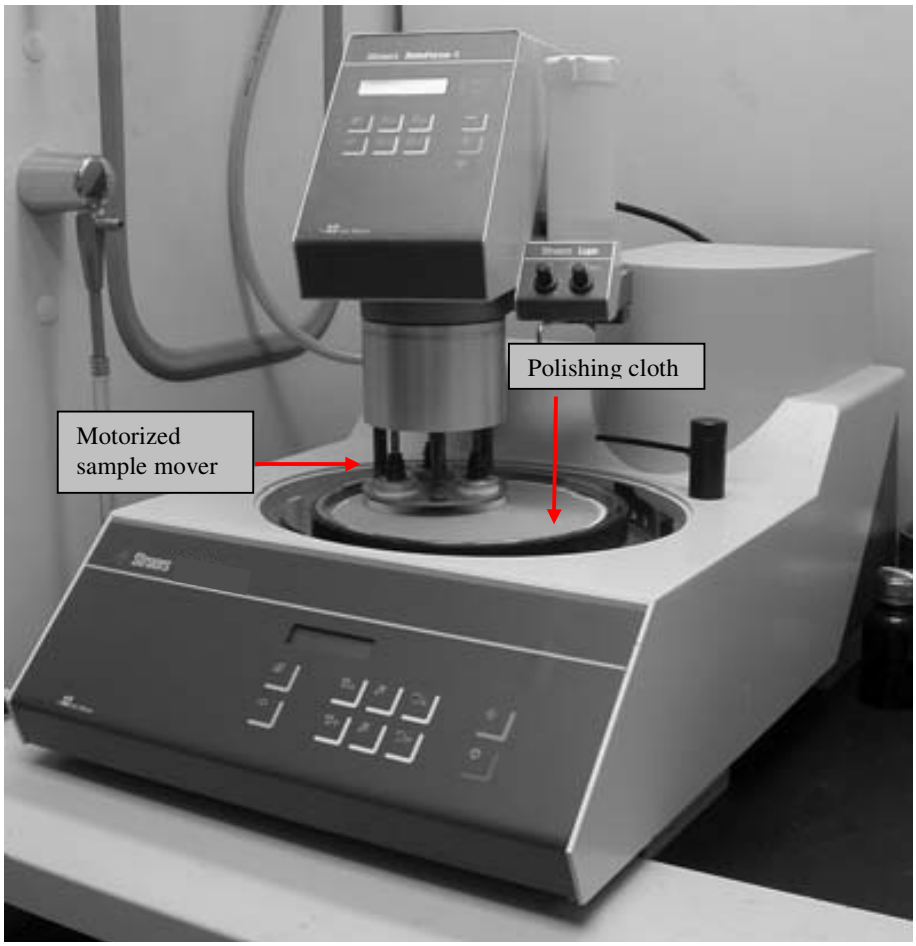

Figure 3.1: Struers Rotopol-22 polishing machine

The polishing was performed using 9 μm, 6 μm, 3 μm diamond slurry followed by alumina suspension. The purpose of the polishing was to get a smooth surface and to obtain a better adhesion between coating and substrate. The roughness of the polished substrates was determined by AFM to be 0.1 μm. .

Prior deposition the Al substrates were cleaned first in an ultrasonic bath for duration of 5 minutes per each step. Organic compounds such as methanol, acetone, trichloroethylene, de-ionized water and 5 % HF acid were used in this experimental cleaning process. After cleaning the Al substrates were loaded in the high vacuum electron beam evaporator (see fig.3.2) for the deposition of Pt.

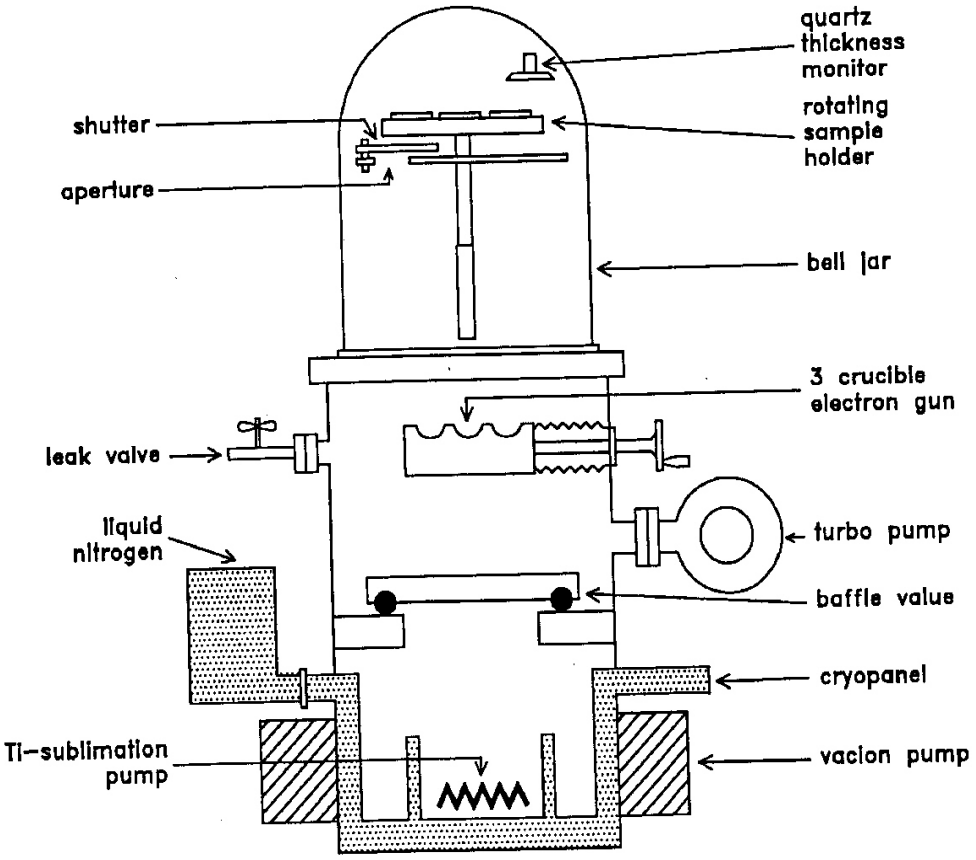

Figure 3.2: Schematic diagram of high vacuum evaporator system used to deposit platinum on aluminium [17].

The temperature of the Al substrates was maintained at approximately 25 °C (room temperature) during deposition. Platinum was heated by a beam of electrons to a point where it started to evaporate and consequently the Pt atoms were stacked on the Al substrate during condensation. Platinum coatings of 0.1 μm and 0.3 μm were deposited on thick Al substrates. The quartz thickness monitor was used to oversee the thickness of Pt coatings. High vacuum was achieved by using different pump systems. A Rotary roughing pump was used to reduce the pressure to about 10^{-1} Torr.

The pressure inside the chamber was then reduced to a pressure of about 10^{-5} Torr by the turbo-molecular pump. The pressure inside the chamber was further improved to 10^{-7} Torr by using liquid nitrogen. A thermocouple gauge was used to measure pressures down to 10^{-2} Torr while a penning gauge was used to measure pressures down to 10^{-7} Torr.

3.1.2 Vacuum annealing

Materials are often heat-treated (annealed) to improve their properties and atomic diffusion occurs during heat treatment. The migration of atoms at elevated temperatures eventually becomes large enough to provide readily observable effects, including changes in chemical composition or atomic distribution. In this work all samples were heat-treated (annealed) in vacuum in a non protective atmosphere. An Elite thermal systems limited furnace was used for all annealing experiments. Samples were placed in quartz boats and loaded into the carousel of the furnace for annealing. Figure 3.3 shows a diagram of the furnace with different parts used for annealing.

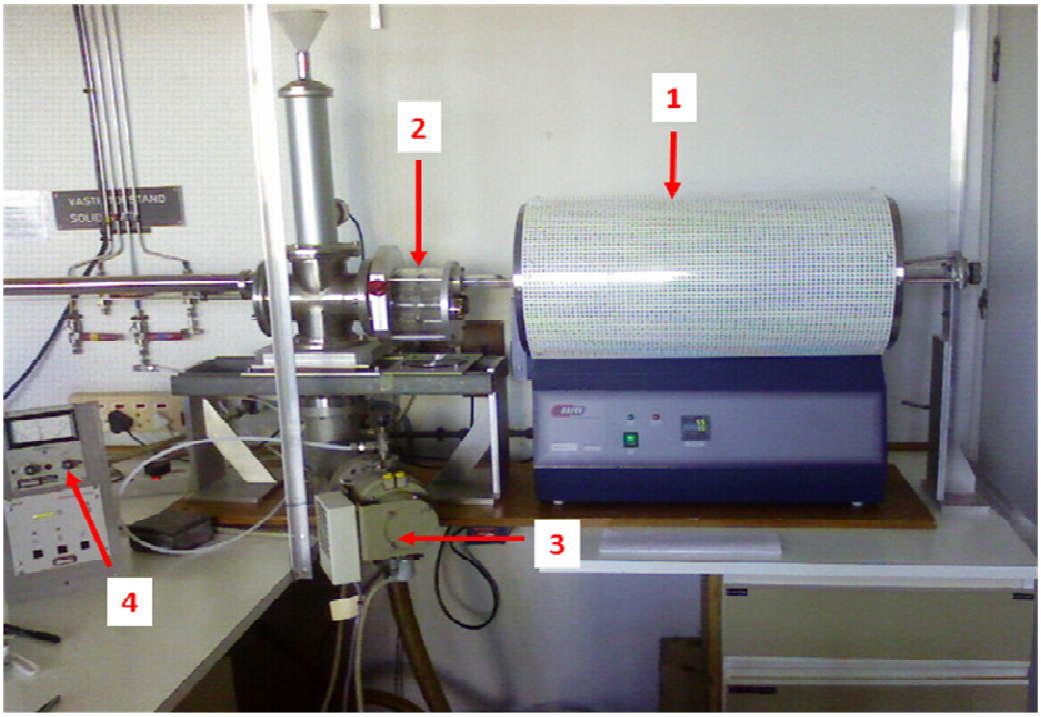

Figure 3.3: Diagram showing important parts of the furnace used for annealing. (1) Furnace, (2) Carousel, (3) Vacuum pumps, and (4) Pressure gauge.

All samples were annealed in vacuum with pressures better than 10^{-7} Torr; vacuum was obtained using a mechanical forepump together with a turbo-molecular pump. The temperature in the furnace was controlled by the microprocessor unit. Samples were annealed at different temperatures ranging from 200-600 °C for the duration of 30 min and an hour. The effects of annealing temperature and time on the coating morphology as a function of coating thickness and formation of Pt-Al intermetallics have been studied. In order to study the changes caused by annealing process several analytical techniques were used and their principles are described in section 3.2 below.

3.2 Characterization Techniques

Pt-Al coated systems in as-deposited and annealed conditions were studied by complementary techniques. The main aim of this work was to study the morphology of the Pt-Al coated systems after annealing at different temperatures and thus, the scanning electron microscope (SEM) and atomic force microscope (AFM) were used to investigate the coatings morphology while the elemental distribution and concentration of elements were determined using particle induced X-ray emission. The formation of Pt-Al intermetallic phases formed during annealing was studied by X-ray diffraction (XRD) technique as well as Rutherford backscattering spectrometry (RBS). The principles of these five techniques are briefly described in this section.

3.2.1 Atomic Force Microscopy (AFM)

The atomic force microscope is a widely used technique with applications in metal coatings. By using the AFM one can be able to image the surface of a sample and determine the roughness of the sample's surface by probing with a tip of the cantilever. The AFM probe tip oscillates at its resonance frequency, while a deflection sensor with a laser-beam focused on the back of the probe constantly measures the amplitude and frequency of the tip **[23]**. Changes of amplitude are transformed into a 3-D picture by means of imaging software. During the scanning process, the probe tip does not touch the sample because the atomic forces reflect the probe tip before a collision occurs **[22, 24].** The AFM scans the surface of the sample with a sharp tip mounted on a flexible cantilever (fig. 3.4). In its contact mode the tip scans the sample in close contact with the surface with a certain force.

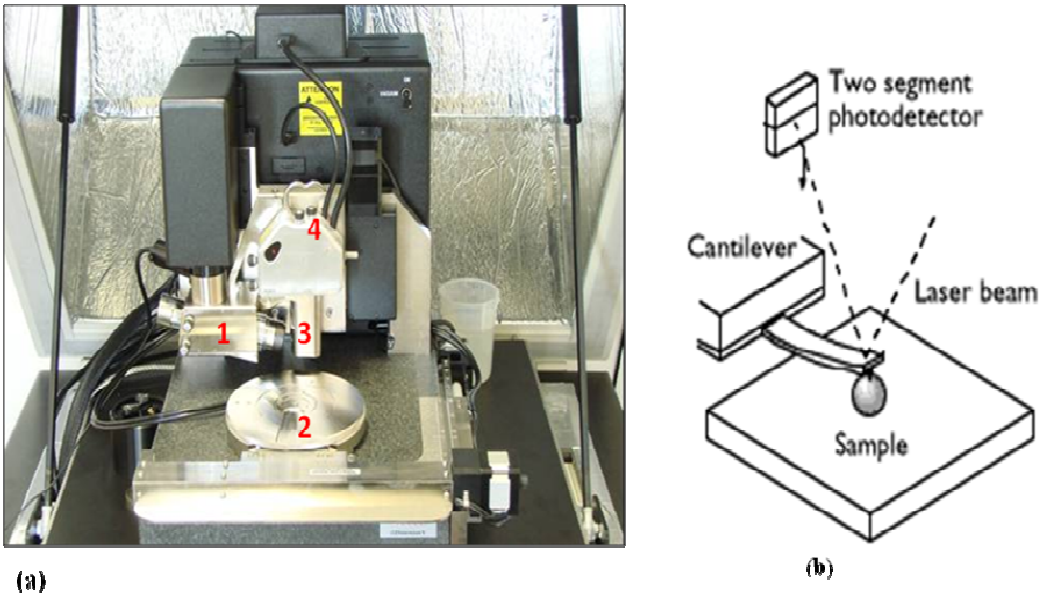

Figure 3.4: (a) The nonoman V atomic force microscope; (1) Optical microscope, (2) sample stage, (3) scanner, (4) laser adjustment knob. (b) Schematic diagram of the atomic force microscopy [24].

The force between the tip and the sample surface is usually less than 10^{-9} N. Electronic feedback loop is used to follow the topography of the sample by adjusting the position of the sample relative to the tip to maintain a constant deflection of the cantilever and thus interaction force. The deflection of the cantilever is measured by bouncing off a laser beam at the back of the cantilever and the displacements with a pair of photosensors. AFM analysis was conducted with a high resolution AFM with imaging system which consists a DI Nanoscope V SPM control station, a Dimension V Scan head with a hybrid XYZ closed loop scanner, a motorized stage with a sample chuck size of 150 mm in diameter, and an optical microscope which provides real-time colour video display at a 1.5 μm resolution with a maximum field of view of 675

μm. Different parts of the sample were scanned and an average scan size of 2 μm × 2 μm was used to obtain the final image.

The atomic force microscope shown in (fig. 3.4) was used for imaging and to determine the surface roughness of the samples. The average surface roughness can be defined as the average distance from the centerline. Figure 3.5 shows a schematic diagram showing the centreline, peaks, and valleys of a sample.

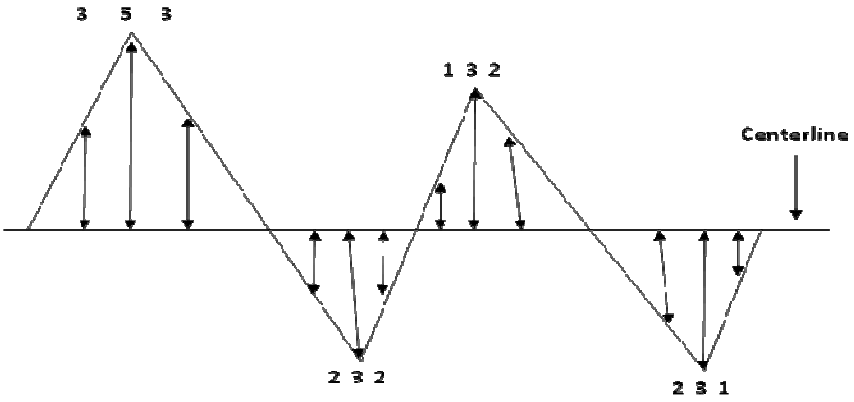

Figure 3.5: Schematic diagram showing heights and depths profiles of a sample.

The centerline (line between surface peaks and valleys) is defined to be the line that divides the profile in a way that the net deviation is zero **[22]**. The roughness average value for a sample with heights and depths as in figure 3.5 is the average value of all the distances from the centerline which gives a value of Ra= 2.5.

3.2.2 Scanning Electron Microscopy (SEM)

The scanning electron microscope is the most widely used technique to study surface morphology, microstructure and chemical composition. The scanning electron

microscope images the sample surface by scanning it with a highly focused beam of electrons**.**

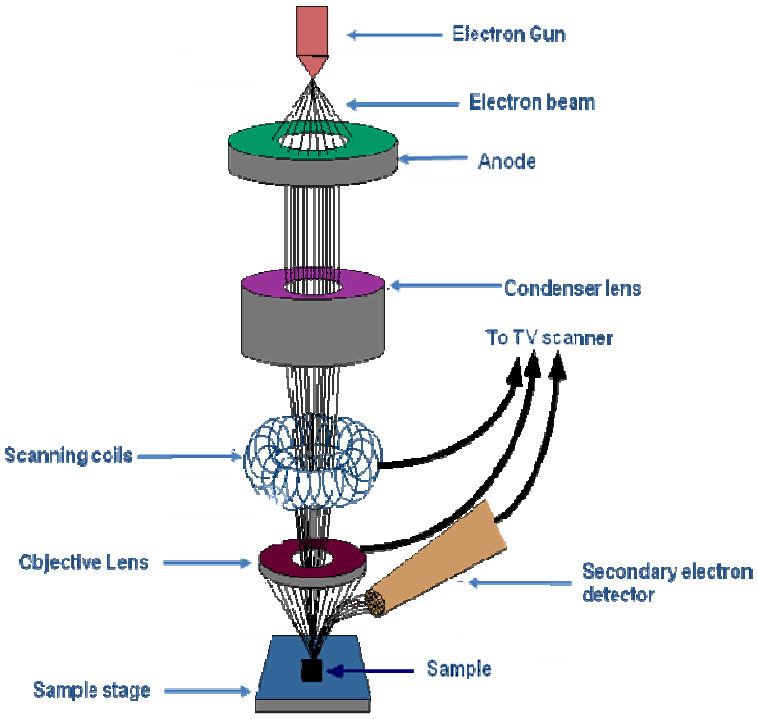

Figure 3.6: Schematic diagram showing the basic components of the scanning electron microscope [26].

Electrons are thermoinically generated from a filament (usually tungsten) and accelerated towards the anode **[26-27]**. The production of electron beam takes place in the electron gun. The beam is then condensed by the condenser lenses. The scanning coils scan the beam in a grid fashion, dwelling on points for a period of time determined by the scan speed. Finally the objective lens focuses the scanning beam onto the preferred part of the sample. Figure 3.6 shows schematic of a scanning microscope. When the beam strikes the sample, interactions occur inside the sample and various signals are generated. The generated signals contain information about the sample being studied. Electronic devices are used to detect and amplify the signals

and display them as an image on a cathode ray tube**.** Figure 3.7 shows numerous signals generated when a primary beam of electrons interact with atoms of a solid specimen **[26-27]**.

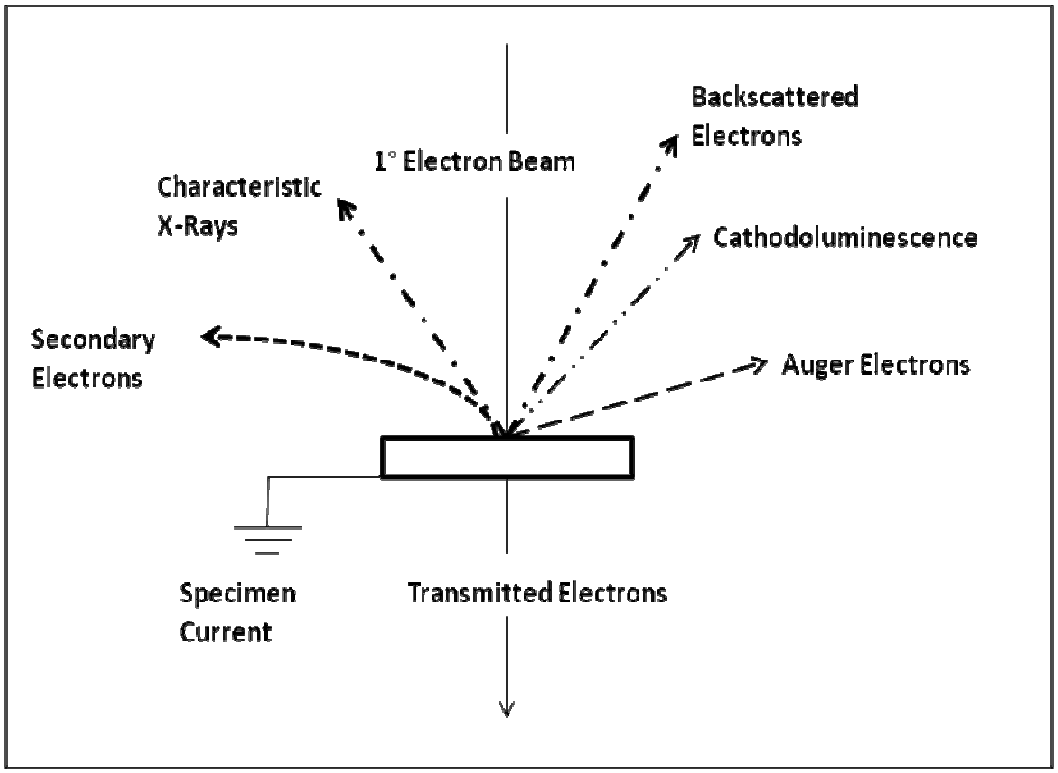

Figure 3.7: A diagram showing possible signals generated when a primary beam interact with a specimen [25].

From the several signals generated during the primary electron beam-specimen interaction, the two signals (i) secondary electrons and (ii) characteristic X-rays were collected by detectors to form the image of the sample on a screen **[26-27]**. These signals come from the beam of electrons striking the surface of the specimen and interacting with the sample at or near its surface. Interactions between the electron beam and the sample's electrons causes shell transitions which results in the emission of secondary electrons by inelastic scattering and the emission of electromagnetic

radiation (characteristic X-rays). During inelastic interactions between incident electrons and sample's electrons, the electrons lose much of their energy and the result of this process is the emission of low energy electrons termed secondary electrons. The secondary electron detector was used to collect secondary electrons which originate from some few nanometers of sample surface with energy less than 50 eV **[26-27].** Secondary electron imaging provides high resolution imaging of surface morphology. The energy dispersive spectroscopy (EDS) is a technique used to determine the elemental composition of the coatings used in this study. This technique is used in combination with the scanning electron microscope. Emitted X-rays have an energy characteristic of the parent elements in the specimen. The energy of the emitted x-rays was measured to detect elements in the material. The surface morphology was studied using SEM (Oxford Stereoscan 440 operated at acceleration voltage of 20 kV and a beam current of 100 pA and at an average working distance of 17 mm).

3.2.3 X-ray Diffraction (XRD)

The X-ray diffraction technique was used in this study to investigate the formation of intermetallic phases formed during annealing in the Al-Pt system. X-ray scattering is used extensively for characterizing the crystal structure of the materials. The measurements are based on the diffraction of the electromagnetic waves. X-rays are electromagnetic waves of high frequency and hence small wavelength. Electrons emitted from the heated cathode by thermionic emission in vacuum are accelerated towards the anode (target) by a large potential difference V **[28-32]**.

The projectile electron interacts with either the orbital electrons or the nuclei of the target atoms. The interactions result in the conversion of kinetic energy of the projectile electron into thermal energy and electromagnetic energy in the form of X-rays **[28, 29]**. X-rays are produced in the X-ray tube and directed to the sample. A position sensitive detector was used to detect diffracted X-rays. In this configuration the detector and the X-ray tube move in a locked coupled mode. This mode is usually called a θ-θ scan mode **[33]**, the detector move angle θ for each θ the X-ray tube move while the sample is kept in a fixed position. Figure 3.8 shows the image of a Bruker Advance 8 X-ray diffractometer. The X-ray tube was operated at voltage of 40 kV and a current of 40 mA.

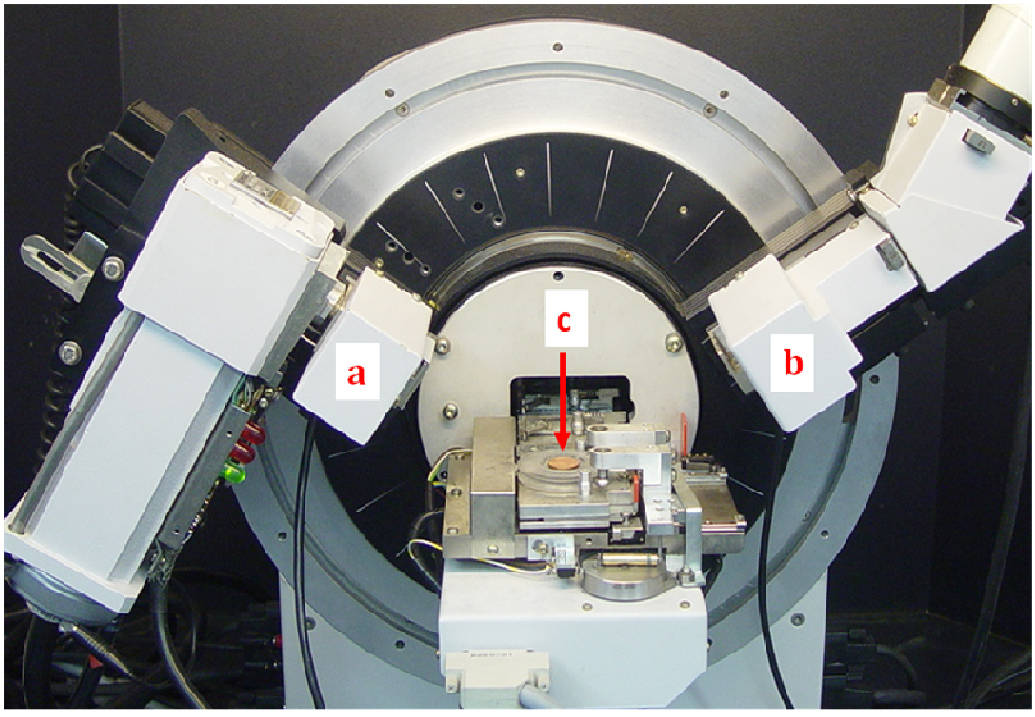

Figure 3.8: Bruker Advance 8 X-ray diffractometer. (a) X-ray tube, (b) Detector, (c) sample stage.

When a monochromatic X-ray beam with wavelength λ, on the order of lattice spacing d, is projected onto a crystalline material at an angle θ, X-ray diffraction patterns are produced by constructive interference of monochromatic beam scattered from each set of lattice planes at specific angles. Constructive interference gives the diffraction peaks according to Bragg's law **[28-29]**;

$$2d\sin\theta = n\lambda \tag{3.1}$$

where d is the distance between adjacent crystal planes, λ is the wavelength of incident X-rays, the integer number n=1, 2, 3… is called order of diffraction.

To satisfy this condition the two parallel rays that strike the diffraction plane must interfere constructively. Figure 3.9 shows two parallel rays reflected by atoms in a crystal. There will be a path difference between the ray reflected at A and the ray reflected at D, if this path difference is equal to any integer number of wavelength then the two separate waves will arrive at a point with the same phase, thus undergoing constructive interference **[28-29]**. When these geometric requirements are met, a diffraction pattern is produced. In a diffraction pattern X-ray intensities are recorded as a function of 2θ angle. By plotting the intensities and positions (2θ angles) of the resultant diffracted peaks of radiation produces a pattern, which is a distinctive feature of the material being studied.

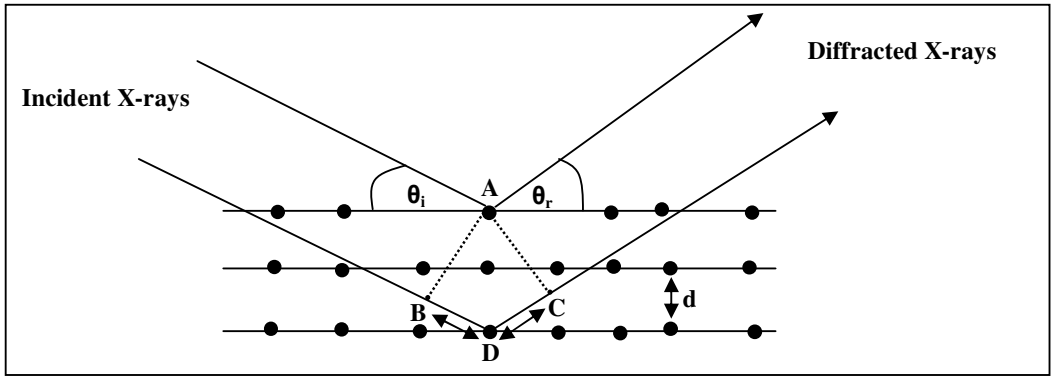

Figure 3.9: A schematic showing specular reflection of two parallel X-rays after interaction with atoms in a sample [28].

The phase analyses in this research have been performed using CuKα radiation (wavelength (λ≈1.54 Å). X-rays measurements were performed between 2θ range of 20-110° with a step size of 0.03°. The international center for diffraction data (ICDD) 1998 database was used to identify diffraction peaks of corresponding Pt-Al phases.

3.2.4 Particle Induced X-ray Emission (PIXE)

The particle induced X-ray emission is a technique in which X-rays emitted during particle and sample interaction are used for elemental analysis. Particle induced X-ray emission is a technique that is used for elemental analysis **[34]**. The analysis is based on: (i) determination of elements present in a specimen by energies of the characteristic X-rays, and (ii) quantitative analysis to identify the amount of each and every element present in the specimen. PIXE offers better peak to noise ratios and consequently much higher trace element sensitivities which makes it special compared to electron based X-ray analytical techniques such as energy dispersive spectroscopy (EDS) **[34]**. A beam of protons is used in this technique to knock out electrons from the one of the shells in the target and cause atoms in the target not to

be stable. Quantum theory states that orbiting electrons of an atom must occupy discrete energy levels in order to be stable. Bombardment with ions of sufficient energy (usually MeV He^{++}) will cause inner shell ionization of atoms in a specimen. Outer shell electrons drop down to replace inner shell vacancies, however only certain transitions are allowed. X-rays of a characteristic energy of the element are emitted **[34-36]**. An energy dispersive detector was used to detect and record X-rays and these X-rays were then converted to elemental concentrations. Figure 3.10 shows the creation of a vacancy in a K-shell.

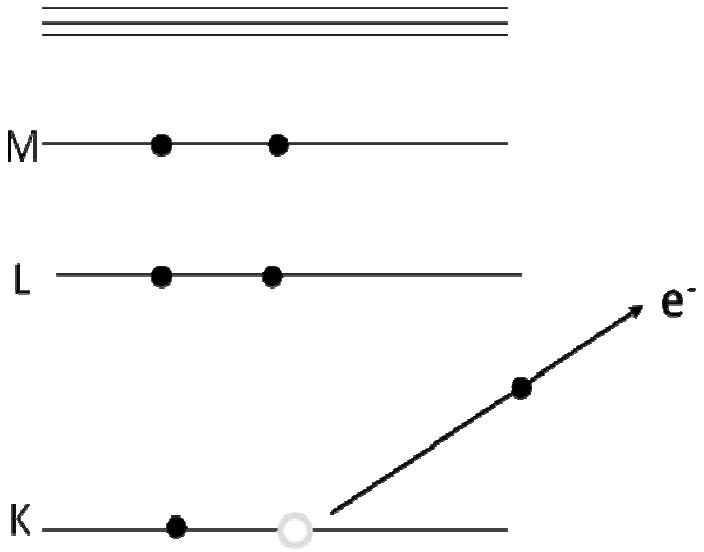

Figure 3.10: Removal of an electron from the K shell during particle and sample interaction creating a vacancy [34].

Characteristic X-rays are produced during the stabilization process when an electron from high energy shell fills the vacancy created in the lower energy shell (see fig. 3.11). The filling of the vacancy can be from different energy levels and the emission of electromagnetic radiation in the form of X-rays characteristic of the excited atom is

a consequence of this process. The X-rays emitted when electrons fall back into the core hole can be used to identify each element within the sample.

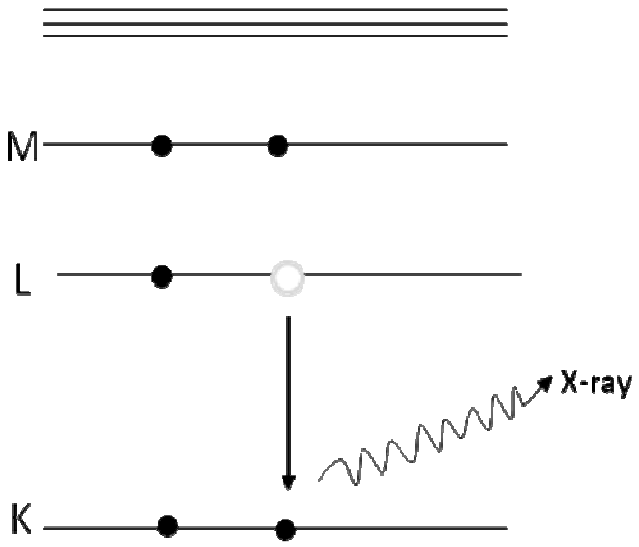

Figure 3.11: Electron from higher energy shell filling a vacancy in a lower energy shell producing some x–rays in the process [34].

Figure 3.12 shows some features inside the nuclear microprobe experimental chamber. Highly focused ion beam used for analysis was produced from the Van der Graaff accelerator. A focusing system that consists of collimators and magnetic quadrupoles was used to focus the ion beam into the experimental chamber. The experimental chamber accommodates (i) a sample stage, (ii) optical microscope, (iii) filter wheel and the (iv) Si(Li) detector as well as several radiation detectors. Samples were mounted and positioned on a sample stage with 3-degrees of freedom of movement (x, y, z axis movement). The sample was viewed by an optical microscope at an angle of 45° with respect to the sample.

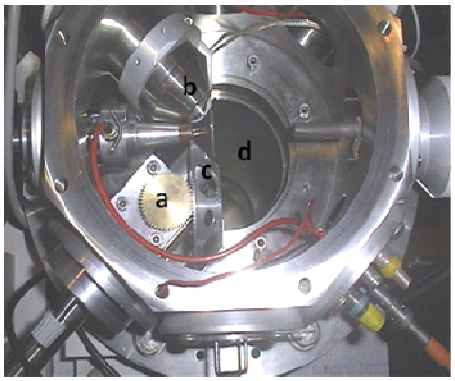

Figure 3.12: The inside of the experimental chamber. (a) Si(Li) detector, (b) optical microscope, (c) filter wheel , (d) sample stage.

A *2* MeV beam of alpha particles was used to probe a sample area of 0.5 × 0.5 mm^2 with a beam spot size of 3 × 4 μm^2. This investigation was carried using a beam current of approximately 100 pA. An ion beam at an incident angle of 0° was directed to the sample. The Princeton Gamma Tech (PGT) Si (Li) detector placed at an angle of 45° from the sample was used to record emitted characteristic x-rays after the interaction between the beam of alpha particles and the samples. The software package Geo PIXE II was used reconstruct elemental maps from characteristic X-rays of the elements detected on the surface and sub-surface of the Pt coatings.

3.2.5 Rutherford Backscattering Spectrometry (RBS)

Interdiffusion studies and possible interactions under various annealing conditions in the Al and Pt system were carried out using RBS. Rutherford backscattering spectrometry is based on classical scattering in central-force field and for this reason is easy to understand and to apply it. Ions of few MeV energy were focused at normal

incidence into the specimen surface and the energy of particles scattered through an angle θ was measured by a nuclear particle detector **[35-37]**. The typical experimental setup is shown in figure 3.13.

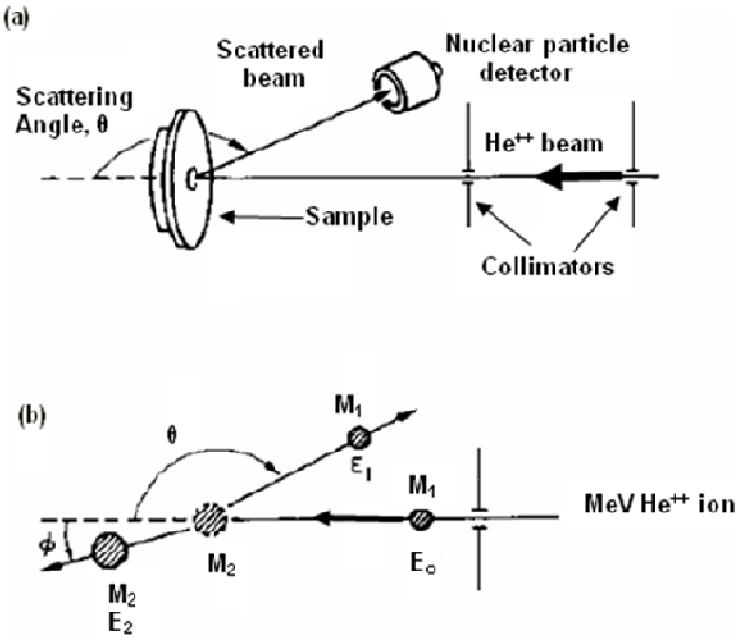

Figure 3.13: (a) Experimental setup for RBS technique. A beam of 2 MeV ions is directed to a sample. Particles scattered by target atoms are detected by a nuclear particle detector. (b) Schematic showing elastic collision between nucleus of incident atoms and nucleus of target atoms [37].

Scattering occurs between the nucleus of the incident ion and the nucleus of the target atom **[34-37]**. During collision energy is transferred from the projectile to the stationary target atom, this energy transfer provides the signature of the target atom. Equation 3.2 **[17, 37]** shows the energy ratio (kinematic factor) of the incident ion and target atom.

$$K = \frac{E_1}{E_0} = \left[\frac{\left(M_2{}^2 - M_1{}^2 \sin^2\theta\right)^{\frac{1}{2}} + M_1 \cos\theta}{M_2 + M_1} \right]^2 \qquad (3.2)$$

where E_0 and E_1 are the energies of the incident particle before and after collision respectively. M_1 and M_2 are the masses of the incident and target nuclei respectively. The angle θ is the scattering angle.

When an incident particle penetrates a target some of its energy will be lost during its trajectory to the electrons of the target atoms by ionization and excitation as well as nuclear collisions. That energy lost in penetration is directly proportional to the thickness of the material traversed so that a depth scale can be assigned directly and quantitatively to the energy spectra of detected particles. To measure this energy loss one must first determine the distance Δt which the particle traversed in the target and the energy ΔE loss in this distance. The energy loss per unit length is expressed as a stopping power, $\frac{dE}{dx}$.

For small energy loss, generally the stopping power ($\frac{dE}{dx}$) does not change much and exist a linear relation between energy loss (ΔE) and depth (t) that can be expressed as $\Delta E = [S]t$, the proportionality factor $[S]$ is called the backscattering energy loss factor. For very thin target film, it can be assumed that $\frac{dE}{dx}$ of the projectile does not change and can be evaluated at the energy E_0 for its incoming route and $E_1 = K E_0$ for its outgoing route. Equation 3.3 **[35-37]** is an expression for the energy lost by a projectile of mass M_1 which was backscattered by an atom of mass M_2 at depth t.

$$\Delta E = [S]t = \left(\frac{K}{\cos\theta_1} \frac{dE}{dx}\Big|_{E_0} + \frac{1}{\cos\theta_2} \frac{dE}{dx}\Big|_{KE_0} \right) t \qquad (3.3)$$

where θ_1 and θ_2 are the angles between the surface normal and the outgoing particle direction respectively.

In a target that contains more than one element (compound target) the energy lost is the sum of the losses of the constituent elements weighted by the abundance of the elements. This postulate is known as Bragg's rule which state that the stopping cross section $\varepsilon^{A_mB_n}$ of a compound A_mB_n is given by **[17 , 37]**:

$$\varepsilon^{A_mB_n} = m\varepsilon^A + n\varepsilon^B \qquad (3.4)$$

where ε^A *and* ε^B are the stopping cross sections for atomic constituents A and B. The energy loss for a particle backscattered from element *A* and *B* at depth t in compound A_mB_n is given in the same way as equation 3.3, the kinematic factor *K* must be substituted by the kinematic factor K_A for element *A* and K_B for element *B*.

The investigation of interaction on the annealed Al-Pt coatings was performed using a 2 MeV beam of Helium ions (He^{++}) 10° tilt. The RBS spectra were obtained using a surface barrier detector with energy resolution of approximately 15 KeV placed at an angle of 165º with respect to the incident beam. The Rutherford Backscattering Utilities and Manipulation Program (RUMP) was used to analyze RBS spectra.

The groundwork and principles required for performing surface coating morphology and phase formation measurements has been laid in this chapter. The present chapter was devoted in providing theoretical framework and principles of the techniques used

in this study and chapter 4 proceeds with presentations and discussions of all the experimental results.

CHAPTER 4 RESULTS

4.1 Surface Morphology Characterization

4.1.1 Atomic Force Microscopy

The surface morphology of the coatings was examined using the atomic force microscope; fig. 4.1 shows the three- dimensional representations of the AFM images for as-deposited 0.1 μm and 0.3 μm Pt layers. This three-dimensional representation allowed us to have a better view of the sample as well as topography of deposited Pt layer. The Pt during the deposition process was heated to its evaporation temperature and during condensation it solidifies on the substrate forming splats. Splats were clearly visible on the AFM images, these splats represents nothing but frozen Pt on the substrate. The splats size was observed to vary between 300 nm and 400 nm range. With AFM it was also possible to obtain quantitative results about the surface roughness. The surface roughness of the as-deposited Al-Pt sample was varying between Ra = 40.50 nm and Ra = 46.23 nm. The surface roughness for both coated systems (0.1 μm and 0.3 μm Pt layers) in as-deposited condition was very similar as shown in fig. 4.1 (a) and (b)).

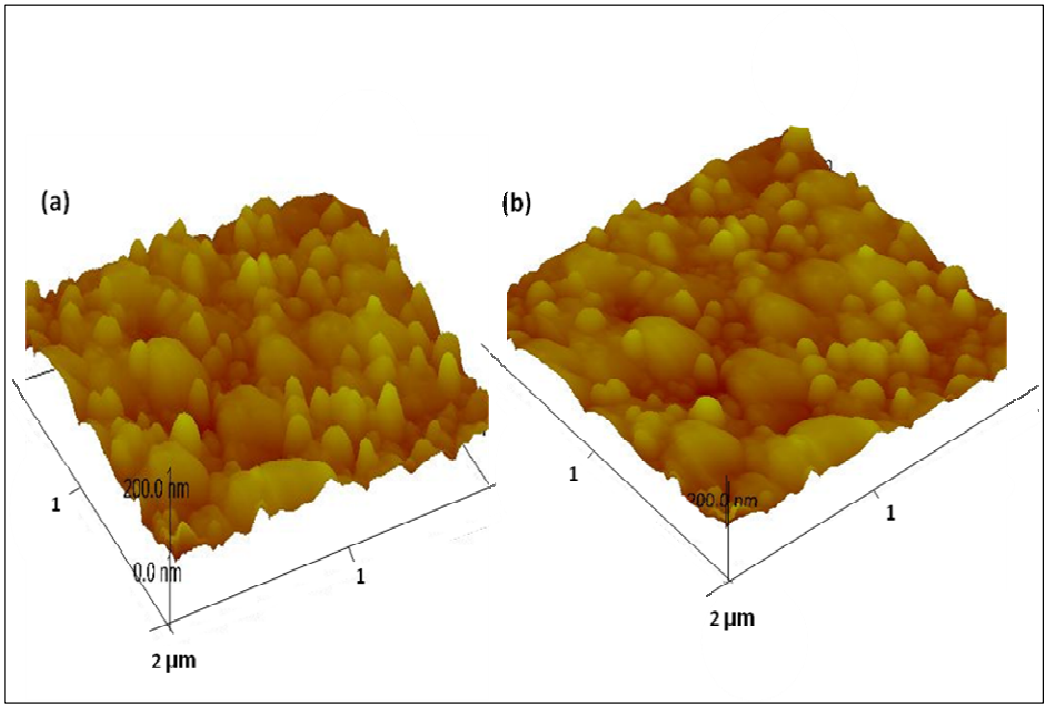

Figure 4.1: 3-D AFM images showing coating morphology of as-deposited Al-Pt coated samples. (a) 0.3 µm Pt layer and (b) 0.1 µm Pt layer.

Table 4.1 shows the surface roughness of as-deposited Al-Pt coated samples obtained in different areas of 2 µm × 2 µm. The roughness measurements were obtained in different as-deposited samples and an average surface roughness of Ra = 43.26 nm was obtained.

Table 4.1: Average surface roughness of as-deposited Pt-Al coated system.

Scanned areas	**Roughness *Ra*(nm)**
1	45.30
2	40.50
3	41.01
4	46.23
Average *Ra*	43.26

.

4.1.2 Scanning Electron Microscopy

The scanning electron microscopy was used to study the effects of annealing parameters (temperature and time) and coating thickness on the morphology of Al-Pt coated systems. Figures 4.2 - 4.11 show the changes in coating morphology of the 0.1 μm and 0.3 μm Pt layers deposited on Al substrates after being annealed. The samples were annealed at temperatures ranging from 200 °C to 590 °C for annealing periods of 30 min and 1 hour. The surface morphology of the as-deposited 0.1 μm Pt coating shows a uniform surface without any obvious surface defects shown by the (fig. 4.2).

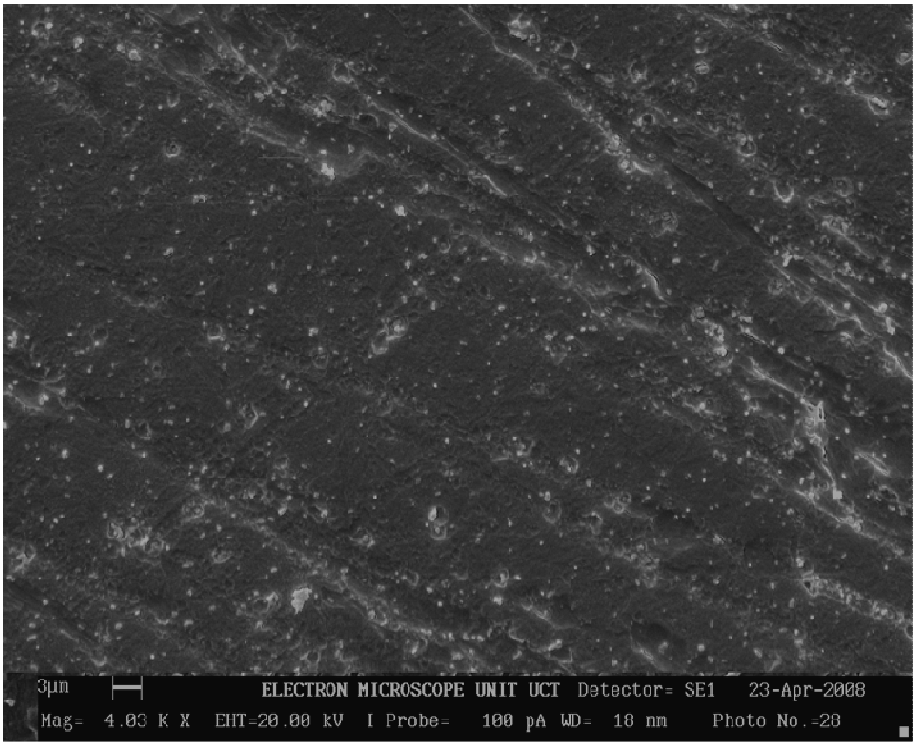

Figure 4.2: SEM micrograph of the as-deposited 0.1 μm Pt coating.

The SEM micrographs in fig.4.3 show different morphologies of thin platinum coatings (0.1 μm) after heat treatments at 200 °C and 400 °C. The coating surface appeared quite smooth after annealing at 200 °C (fig 4.2 a) while a slight change in

surface morphology has been observed after treatment at 400 °C. The effective interaction between elements (Pt and Al) resulted in the formation of intermetallic compounds which upon their growth changed the morphology of the coating.

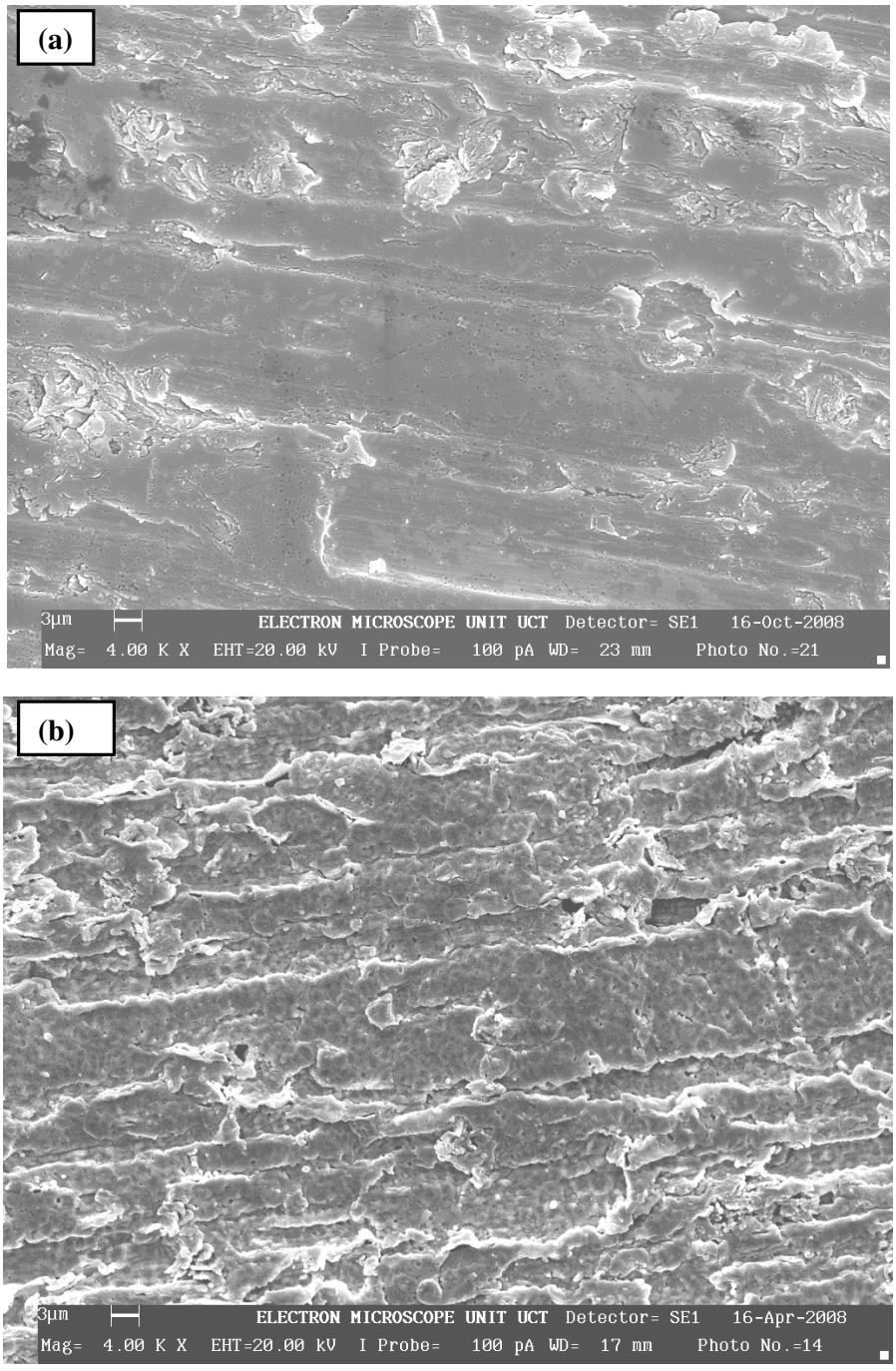

Figure 4.3: SEM micrographs of the 0.1 µm Pt layer annealed for 30 min at: (a) 200 °C and (b) 400 °C.

The microscopical studies showed that the surface morphology of the 0.1 μm Pt coatings changed significantly after annealing at high temperatures of 500 °C and 560 °C (fig 4.4). The surface of the coatings became more uneven (rough) when annealing was performed at higher temperatures. The mismatch in coefficients of thermal expansion of Al and Pt is one of the reasons which contribute to increased surface roughness **[38]**. The two materials do not expand and contract in the same way during heating and cooling: The thermal expansion coefficients (at room temperature) are $23\times10^{-6}/^{o}C \quad and \quad 9.1\times10^{-6}/^{o}C$ for platinum and aluminium respectively **[20]**. In addition, different Pt/Al intermetallic compounds have different mechanical properties and they can induce the residual stresses (tensile or compressive) in coated system. And therefore, all these factors affect the morphology of coated systems subjected to annealing conditions.

Further comparison has been made between coating morphologies at the temperatures close to the Al melting temperature. The system of thin Pt layer (0.1 μm) deposited onto Al substrate has been annealed at 500 °C and 560 °C (fig 4.4). As expected, the microscopic study showed significantly higher surface roughness in comparison to the samples annealed at 400 °C and below. However, it is interesting to point out that the orientation of the coated layer (as shown by arrow, fig.4.4) with respect to substrate was still observed.

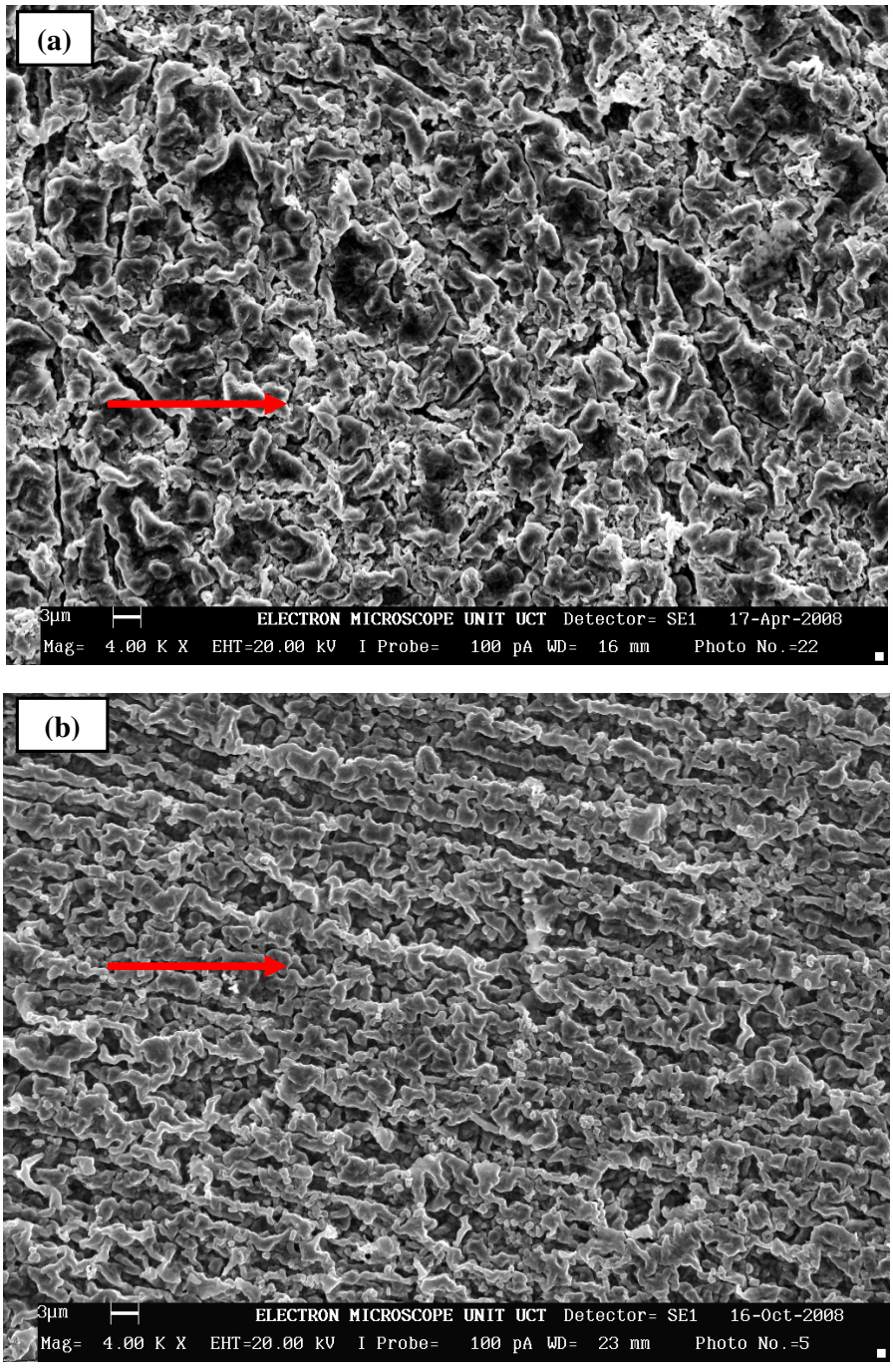

Figure 4.4: Coating morphology of the 0.1 µm Pt layer after heat treatment at (a) 500 °C and (b) 560 °C for 30 min.

The SEM micrographs of the 0.3 µm Pt layer were obtained for the 200 °C and 400 °C heat treated samples (fig. 4.5 (a) and (b)). The surface morphologies of the two

samples looked different. It can be seen that the surface of the 200 °C annealed sample is not smooth, with obvious defects such as cracks as evident in fig. 4.5 (a) while a 'coiled like' surface was observed on the 400 °C annealed sample. It was expected to observe different surface features between these two samples since at 400 °C there was formation of the Al_2Pt and Al_6Pt intermetallic phases as confirmed by XRD. The dependants of surface features like roughness on the manner in which phases grow in a system was reported by Li *et al.* **[43]**. On their work on PtSi/Si system they find that the film roughness was clearly due to the manner in which the PtSi grow.

The 0.1 μm Pt coatings heat treated under same annealing conditions with the 0.3 μm Pt coatings exhibited different surface features. This is an indication of the effect of coating thickness on the surface morphology. It is apparent that the thickness of the Pt layer affects the surface morphology of the coating this is evident on the samples annealed at 200 °C for both 0.1 μm and 0.3 μm Pt layers (fig 4.3 (a) and 4.5 (a)). The two samples were annealed at same temperatures and same annealing time of 30 min but their surface morphology appeared very differently. A smooth surface was observed on the 0.1 μm Pt layer sample while a cracked irregular surface was observed on the 0.3 μm Pt coating.

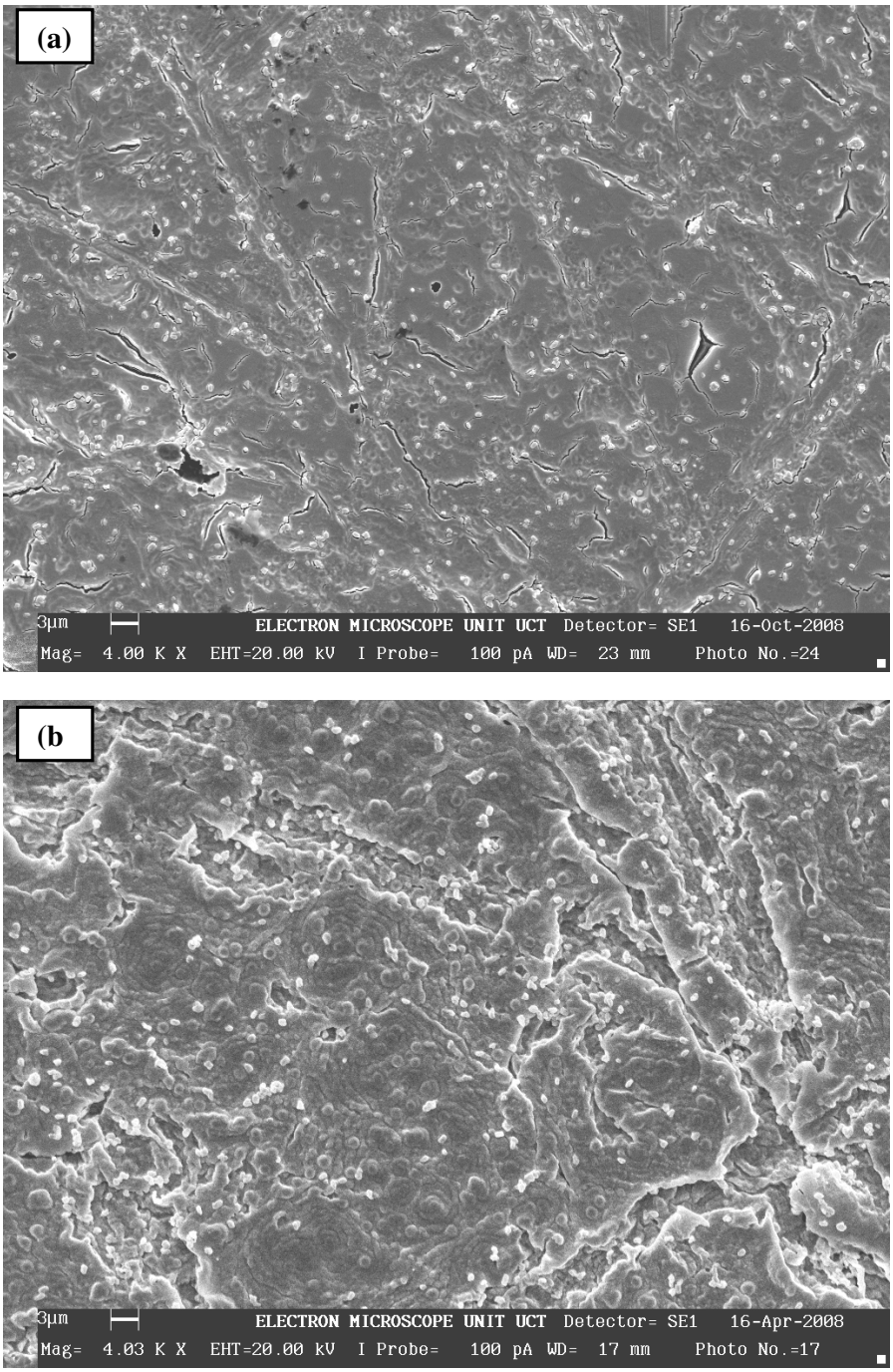

Figure 4.5: Surface morphology of the 0.3 µm Pt layer annealed for 30 min at: (a) 200 °C and (b) 400°C.

Annealing was also carried out at higher annealing temperatures of 500 °C and 560 °C for the same annealing period of 30 min. The SEM micrographs are shown in fig. 4.6.

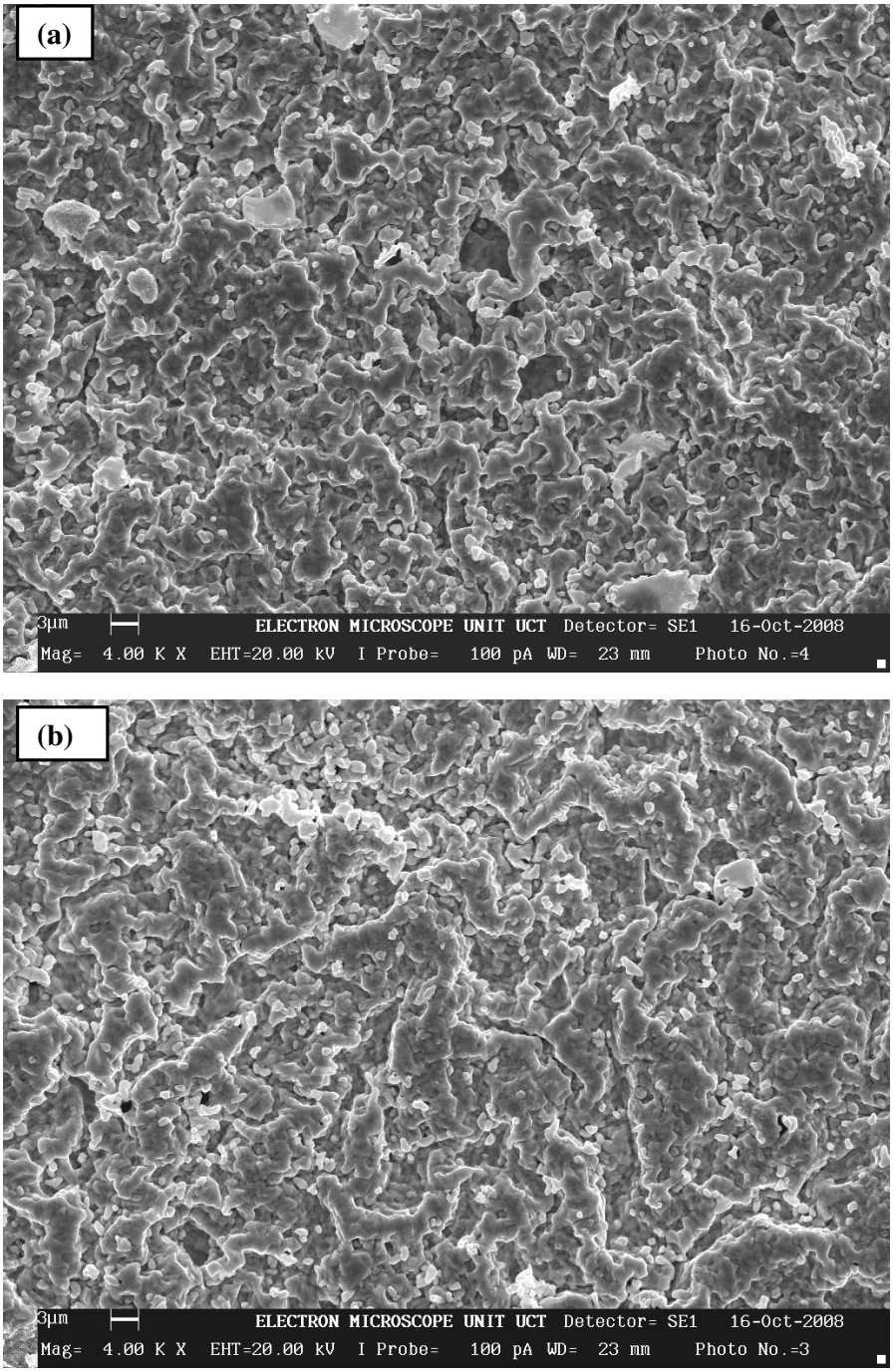

Figure 4.6: Surface morphology of 0.3 µm Pt coating heat treated at: (a) 500 °C, (b) 560 °C for 30 min.

Surface "Wrinkling" which can be defined as a slight ridge in the smoothness of a surface, such as crease caused by surface roughness was observed when annealing at

higher temperatures close to the melting temperature of Al. The results of morphological study are in consistence with the rumpling behavior on the aluminium modified coatings observed by Wen *et al.* **[41]**. The formation of more than one intermetallic phase creates an environment where the reaction rate for each phase is different; and the resulting growth of the phases will be dissimilar **[39]**. This will give rise to uneven surfaces. Surface rumpling is the mechanism which is believed to be responsible for the observed flaws (cracks). The effect of surface rumpling on formation and propagation of cracks has been addressed by Panat *et al.* **[40]** and Wen *et al.* **[41]**.

The microscopical study of the Pt coatings (0.1 μm and 0.3 μm) subjected to annealing temperatures at 500 °C to 560 °C show that high temperature affects the coating morphology of thicker coatings more significantly. The surface of thicker Pt coatings was rougher in comparison to thinner Pt layer subjected to same temperature and time. In addition, the presence of wrinkling and cracking was observed in thicker coatings.

The effects of even higher annealing temperature (590 °C) on morphology of both the 0.1μm and 0.3 μm Pt coated systems are shown in figs. 4.7 and 4.8. The micrograph of the 0.1 μm Pt coating (fig. 4.7) reveals some huge areas on the sample surface without the coating material (region 2 in fig. 4.7). The red arrows in fig. 4.7 indicates very big “islands” of localized coating consumption by the Al substrate. The Pt in these areas was believed to be consumed by the Al which started to melt. Also, interdiffusion between the Pt and Al and subsequent formation of intermetallics are the reasons for extensive consuming of platinum in these regions. Region 1 in fig. 4.7 shows areas on the surface still covered with Pt. PIXE elemental mapping was

performed in micro-regions of the coatings to substantiate the SEM findings. The two techniques showed a very good agreement as they both revealed areas in the coatings with big and small islands indicating the consumption of the coating layer by the substrate material. In agreement with this findings Topić *et al* **[10]** on their work on high temperature study of thin aluminium coatings deposited on thick platinum substrates also reported the consumption of the Al coating by the thick Pt substrate.

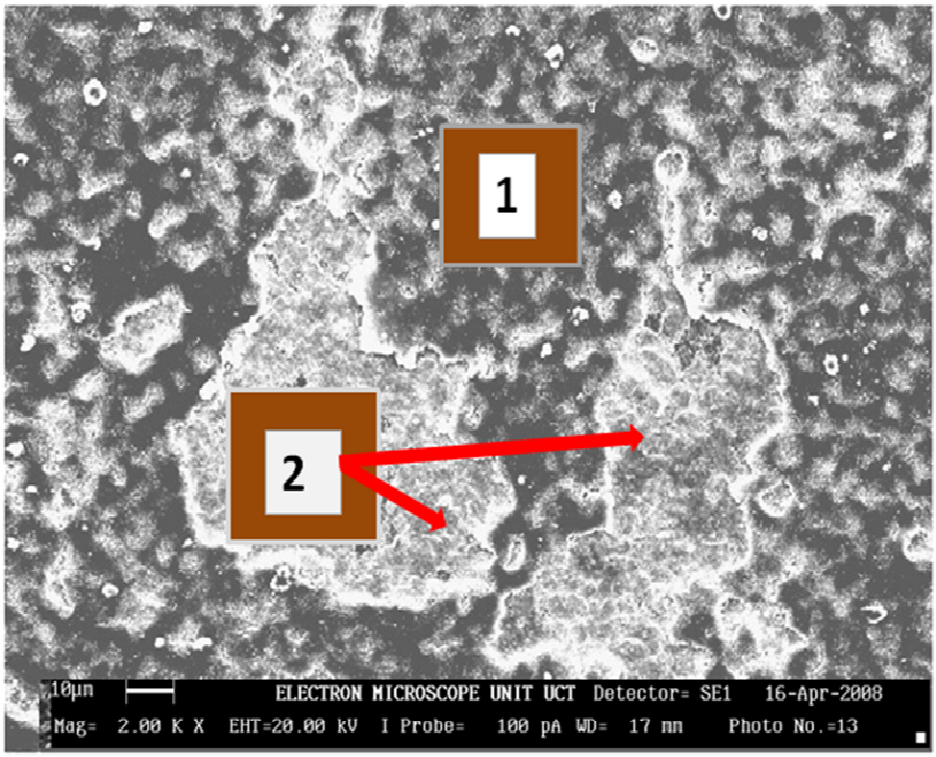

Figure 4.7: Surface morphology of 0.1 µm Pt layer coated samples annealed at 590 °C for 30 min.

For the 0.3 µm thick Pt layer (fig. 4.8) some signs of the coating consumption by the Al substrate were observed (white regions in fig. 4.8). However, the sign of Pt consumption was not as obvious as for the 0.3 µm Pt coating since the Pt layer was thicker. The particle induced X-ray emission technique (PIXE) was also used to investigate this localized coating consumption of Pt by the Al substrate and it was

established that there were islands on the coating surface with complete consumption of the coating material (Pt) by the thick aluminium substrate as evident in fig. 4.15.

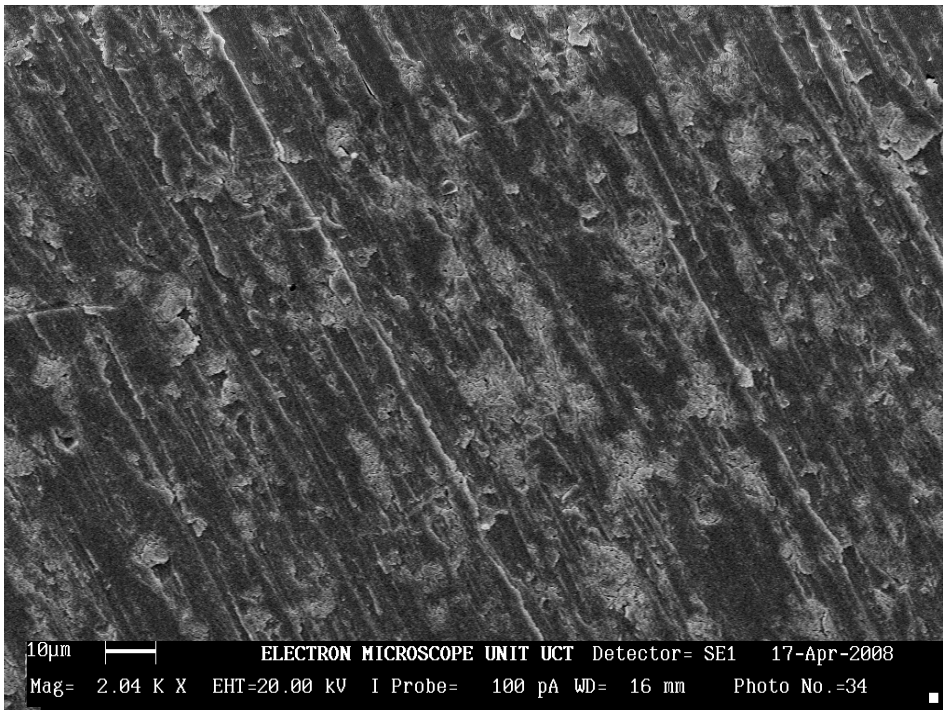

Figure 4.8: Surface morphology of 0.3 µm Pt layer sample annealed at 590 °C for 30 min.

The effect of holding time (annealing period) on the surface morphology of the coatings was another parameter which was investigated in this study. Comparison has been made for both systems (0.1 µm and 0.3 µm Pt layers) annealed at 500 °C in duration of 30 minutes and an hour is shown in figs 4.9 and 4.10. The morphology of the coatings annealed for 30 min exhibit comparable morphology as the coating annealed for 1 hr and this was also the same with the XRD results as almost same intermetallic compounds were observed in both samples annealed for 30 min and 1 hr.

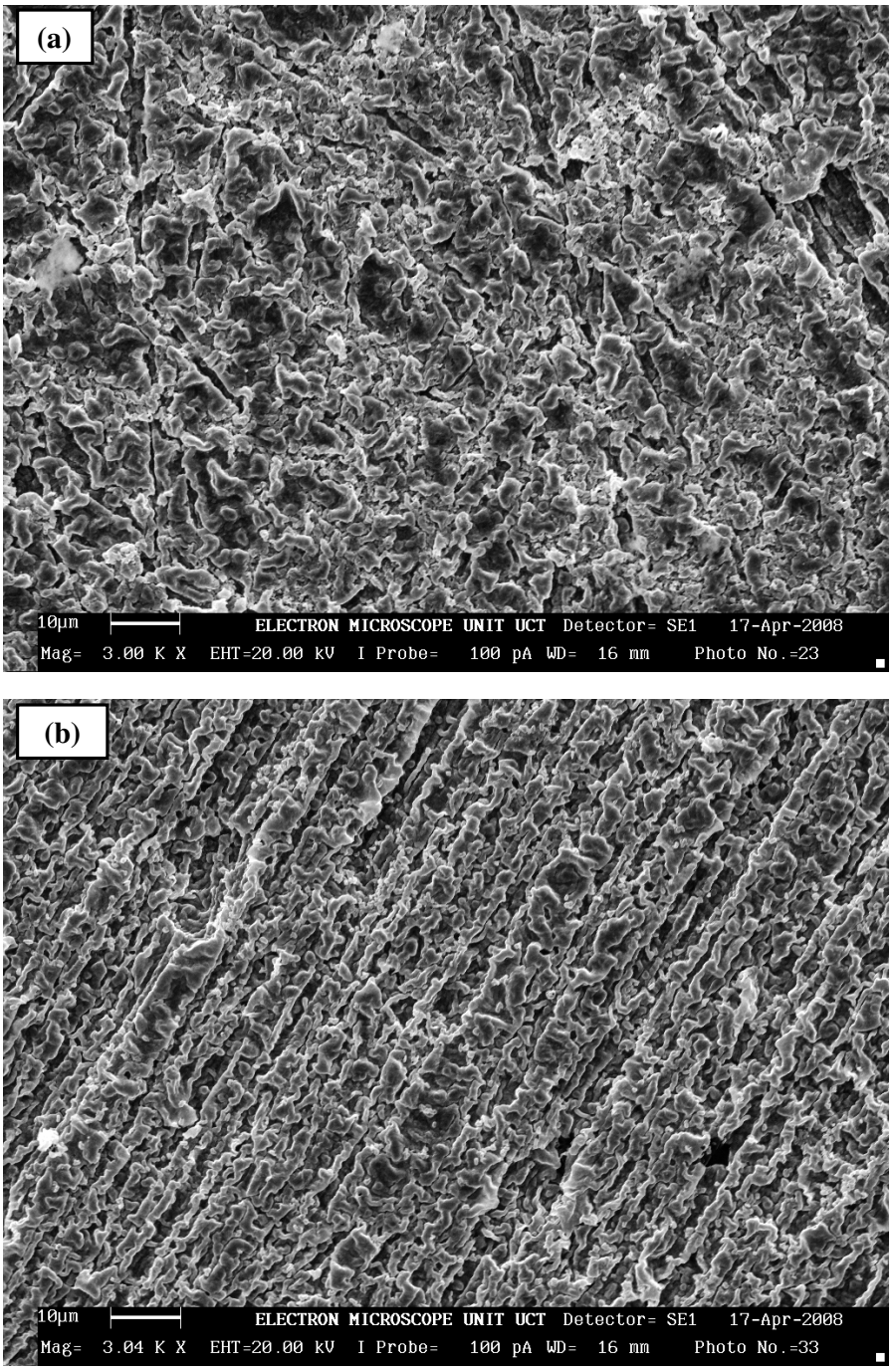

Figure 4.9: SEM micrographs showing coating morphology of 0.1 µm Pt layer after annealing at 500 °C for (a) 30 min and (b) 1hr.

The SEM micrographs in fig. 4.9(a,b) show similar morphology of the 0.1 µm Pt coatings annealed at 500 ℃ in duration of 30 minutes and an hour. The results of

phase analysis show that same intermetallics compounds formed when annealing for 30 min and 1 hr.

The effect of annealing time on the morphology of the 0.3 µm Pt thick coatings was also investigated. The SEM micrographs of the coatings annealed at 500 ℃ for 30 minutes and for an hour are presented in figure 4.10 and 4.11 respectively.

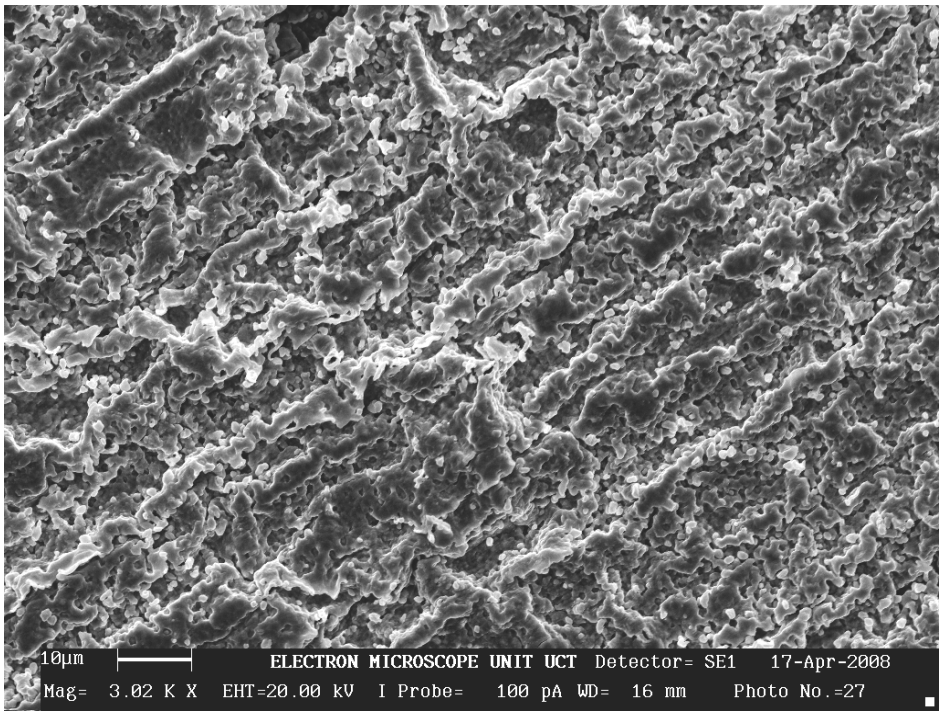

Figure 4.10: SEM micrographs of 0.3 µm Pt coating annealed at 500 °C for 30 min .

By comparing the surface morphology of the sample annealed for shorter time (fig. 410) and the sample annealed for longer time (fig. 4.11), it can be seen the increase of annealing time from 30 min to 1 hr render almost the same surface morphology. However, after annealing for longer time (1 hour) a greater volume of nano size "precipitates" appeared at the surface of the coatings (fig. 411).

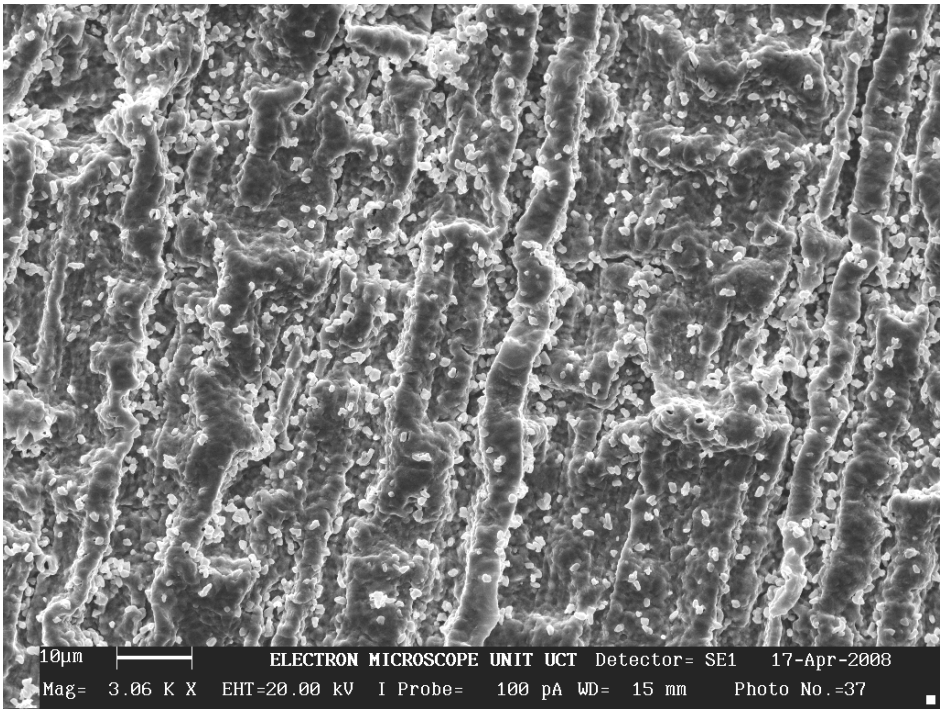

Figure 4.11: SEM micrographs of 0.3 µm Pt coating annealed at 500 °C for 1 hr.

It should be pointed out that the similar morphology has been observed at the coated systems subjected to even higher annealing temperature (590 °C) for 30 min, fig.4.12. High magnification study of the 0.3 µm Pt layer deposited on Al substrate coatings revealed the presence of "small cubical precipitates" (marked by red arrows). An average size of these precipitates was in order of few hundreds nanometers. The formation of precipitates at the topmost layers of the coating was also reported by *Pedraza et al*. **[42]** on their work on platinum-modified aluminide coatings. They found that after aluminisation there were a great number of precipitates at the topmost layers of the coatings which they were discovered to be $PtAl_2$ and Pt_8Al_{21} by XRD.

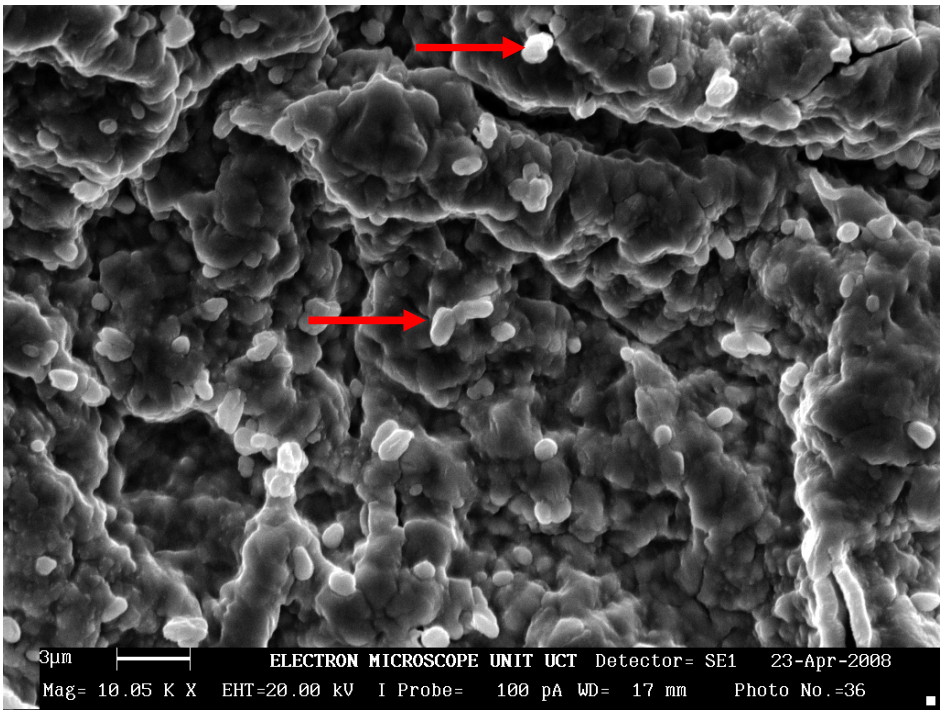

Figure 4.12: SEM micrographs showing the presence of nano size precipitates at the surface of the 0.3 µm Pt layer. Sample annealed at 500 °C for 30 min.

The formation of the "cubical precipitates" has been experimentaly observed in both samples coated with 0.1 µm and 0.3 µm platinum layers. In order to obtain the information about chemical composition of the "precipitates'and relate it with particular phase, the energy dispersive XRD (as a part of scanning electron microscope) has been used. This attempt was made in spite of very small size of the "precipitates" and high penetration of electrons on the coating's surface. Therefore, the X-rays could be collected from the both precipitate and the coating underneath so that they can not be directly related with the formation of phases.

Nonetheless we were able to speculate the elemental constituents of these precipitates using EDS. The areas which are shown by red arrows in fig. 4.12 where there was dominant formation of the spherical crystals were selected and EDS analysis was

performed; only Al and Pt signals were detected in these areas. Since annealing was performed under non-protected atmosphere, the inclusion of other elements like oxygen was of interest in the study. Figure 4.13 shows the EDS spectrum of the 0.3 μm Pt layer sample.

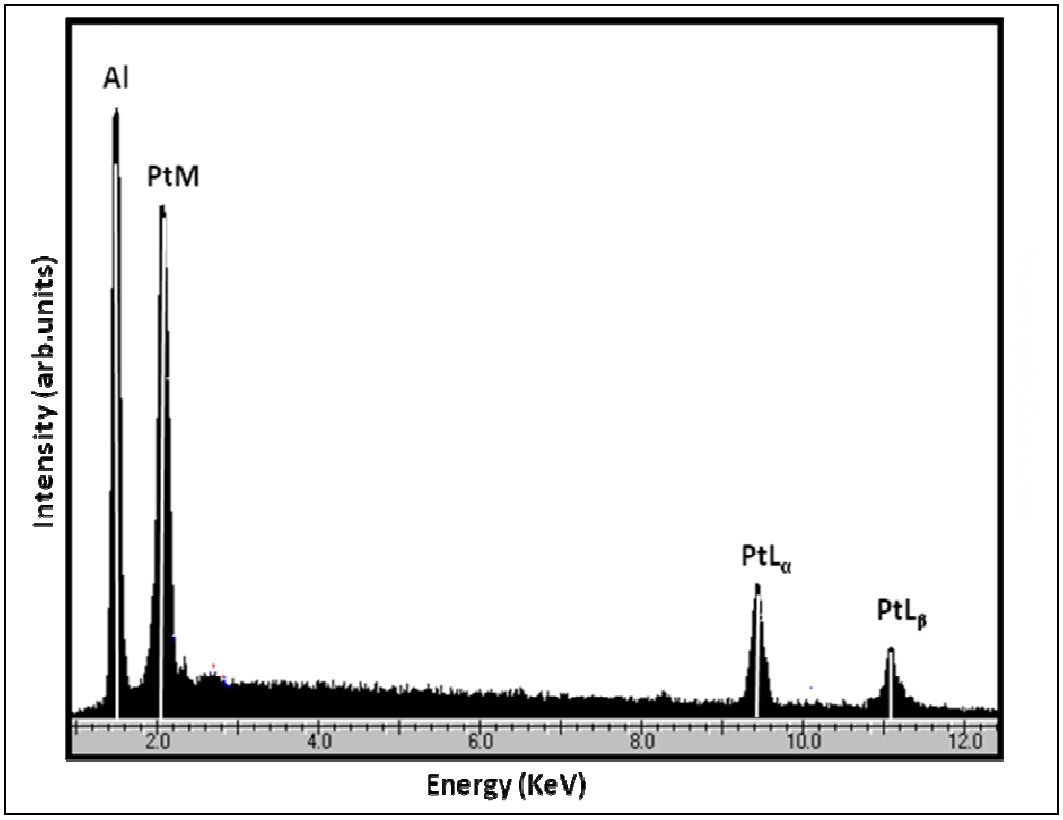

Figure 4.13: Energy Dispersive Spectroscopy spectrum of elements detected on the surface of the coating obtained after bombardment with a highly focused beam of electrons.

Elemental analysis was quantitatively performed and results are presented in Table 4.2. Three selected areas in a sample were of particular interest. By comparing the data in Table 4.2, it can be seen that all the three selected areas render almost the same Al and Pt surface concentrations; an average amount of approximately 64 at.% Al and 36 at.% Pt was determined and we can speculate that it corresponds to the Al_2Pt

($Al_{0.67}Pt_{0.33}$). The intermetallic compound Al_2Pt has been observed by XRD in the samples annealed at temperatures above 350 °C.

Table 4.2: Coating surface elemental composition analysis

Element	Line	Weight%	Error	Atomic%	
Al	Ka	20.02	0.122	64.41	
Pt	La	79.98	0.976	35.59	**area 1**
Total		100.00		100.00	

Element	Line	Weight%	Error	Atomic%	
Al	Ka	19.85	0.103	63.69	
Pt	La	80.15	0.823	36.31	**area 2**
Total		100.00		100.00	

Element	Line	Weight%	Error	Atomic%	
Al	Ka	19.85	0.103	63.78	
Si	Ka	0.22	0.011	0.69	**area 3**
Pt	La	79.93	0.823	35.53	
Total		100.00		100.00	

	Average weight%	Average atomic%
Al	19.91	63.96
Pt	80.02	35.81

In summary, the morphology of thin Pt coatings (0.1 μm*)* heat treated under same annealing conditions as the 0.3 μm Pt coatings exhibited different surface features. The surface of the annealed thin 0.3 μm Pt coatings was greatly affected by surface defects such as cracks as evident in fig. 4.5. Therefore, we can conclude that thickness of deposited coatings play an important role determining the morphology and coating integrity.

The other factor such as annealing temperature is also important factor determining the coating morphology. Higher annealing temperatures promote rougher surface and the formation of cracks. The results of this study show that the time is not so crucial

factor determining the changes in coating morphology. However, the annealing time of 30 minutes and an hour have been only considered in this study.

4.1.3 Elemental composition study by PIXE

The elemental distribution of Al and Pt of the annealed coated systems investigated in this study was mapped out using the particle induced X–ray emission (PIXE) technique. A beam of alpha particles (2 MeV*)* was used to irradiate samples. Figure 4.14 (a, b) shows PIXE maps of Pt and Al of the 0.1 μm Pt coated system annealed at 300 °C for 30 min. As expected, the concentration of Al was low since diffusion rate was low at this temperature (fig. 4.14 (a)). It was found that the Al concentration was varies between 7-14 wt.%. The small concentration of Al originated from substrate material since the Pt layer was very thin (0.1 μm) and the beam of alpha particles penetrated through this layer. The surface of the coating was greatly covered with the coating material (Pt). It was found that the concentration of Pt ranges from 36-45 wt.% (see fig. 4.14(b)). The main feature revealed by the PIXE maps is that interdiffusion between Al and Pt was not effective at 300 °C; these results are consistent with RBS and XRD results as it was observed that there was no interaction at 350 °C and temperatures below.

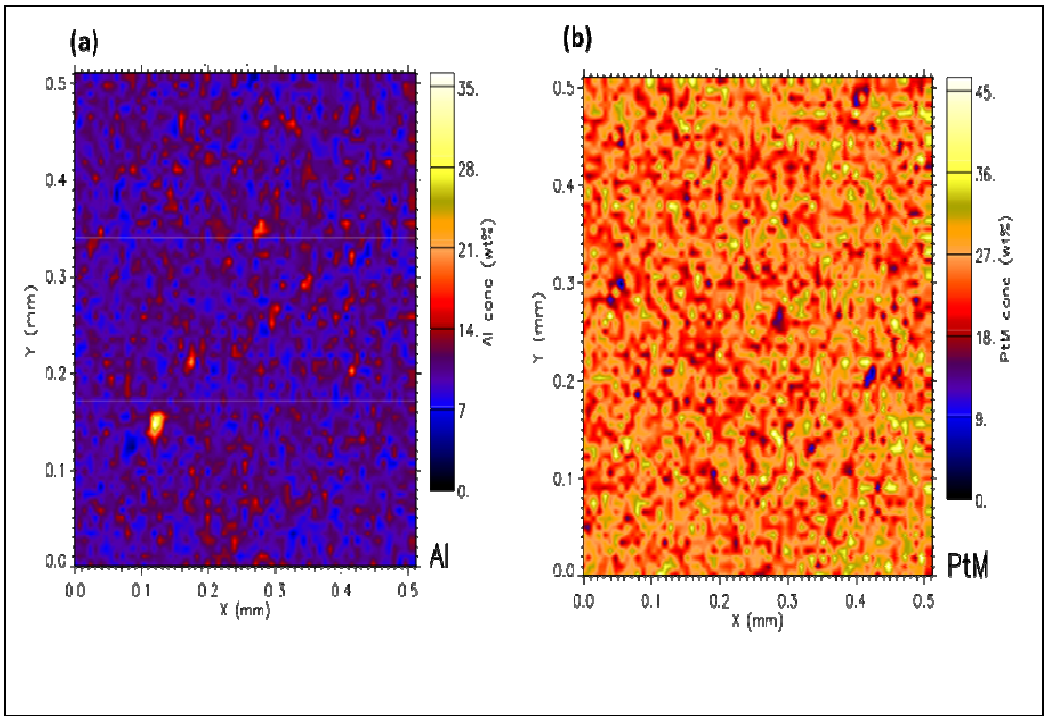

Figure 4.14: X-ray elemental maps collected after irradiation of 0.1 µm Pt thick sample annealed at 300 °C for 30 min with 2 MeV alpha particles: (a) Al map (b) Pt map.

Elemental maps of Pt and Al performed on the sample 0.1 µm Pt layer deposited on Al substrate annealed at 590 °C for 30 min are shown in figure 4.15. The PIXE maps fig. 4.14 (a) shows that the Al concentration varies from 60-80 wt.% in region 1 as shown in fig. 4.15 (a) while a concentration of 20-40 wt.% was found in region 2. In region 1 where the concentration of Al was varying from 60-80 wt.% it was found that the concentration of Pt ranges from 0-20 wt.% (fig. 4.15 (b)). These islands represent the areas where the Pt was fully consumed by the Al substrate and this was also revealed by scanning electron microscopy (fig. 4.7). It is believed that the Al substrate was starting to melt as annealing was performed at temperatures around 600 °C which is very close to the melting temperature of Al (~ 660 °C). The PIXE maps in fig. 4.14 are in a good correlation with the SEM micrographs shown in fig.4.7 as both

are showing the presence of big and small islands on the coating surface. Most area of the surface of the coating was covered by Pt with concentration ranging between 40-60 wt.%. Compared to the sample annealed at 300 °C (fig. 4.13) the surface concentration of Al has increased on the 590 °C annealed sample. The significant increase of Al concentration is attributed to the formation of Al-rich intermetallic phases during annealing at higher temperatures.

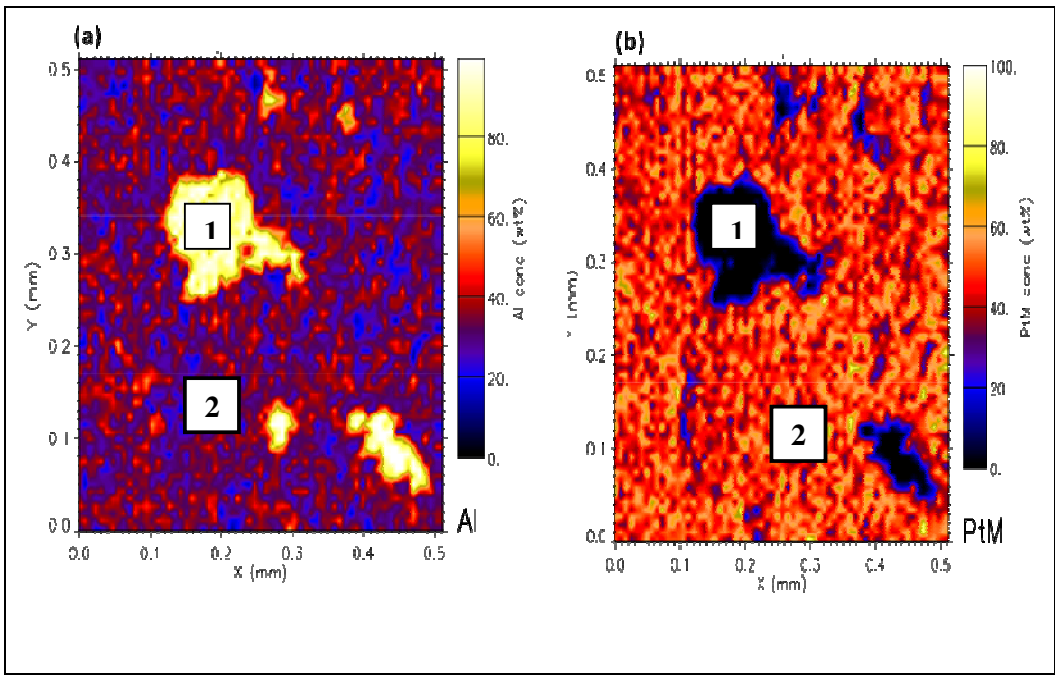

Figure 4.15: X-rays maps for the 0.1 µm Pt layer annealed at 590 °C and irradiated with 2 MeV alpha particles: (a) Al distribution and (b) Pt distribution on coating surface.

Figure 4.15 shows the elemental distribution of the Pt and Al on the 0.3 µm thick coated specimens annealed at 590 °C for 30 minutes. The elemental maps shows a uniform distribution of Al and Pt. It was found that the concentration of Al varies between 30-45 wt.% as shown in fig. 4.16 (a) while the PIXE map for Pt, shows a uniform distribution of Pt with concentration variation between 60 wt.% and 80 wt.%.

It has been seen that the concentration of Al was significantly increased with annealing temperature (comparison between 300 °C and 590 °C). The formation of Al rich intermetallic phases at elevated temperatures ~ 590 °C can be used to explain this increase in Al concentration. In the thinner Pt coating (0.1 µm) the Pt was completely consumed by Al in some areas of the surface leaving the coating surface with Al dominance, but for the 0.3 µm Pt thick coating the were no areas of the coating where there was complete consumption of the Pt since the Pt layer was thicker.

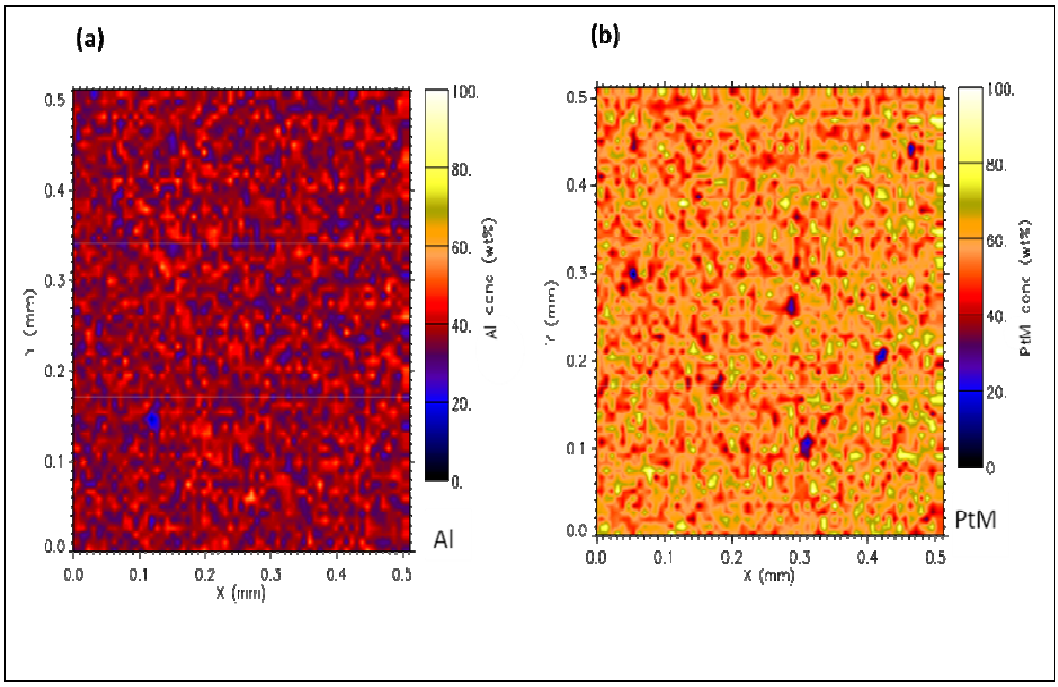

Figure 4.16: PIXE maps for the 0.3 µm Pt thick layer annealed at 590 °C for 30min obtained after irradiating sample with 2 MeV alpha particles.(a) Al map (b) Pt map.

In summary, the microscopy (atomic force microscope and scanning electron microscope) was used to investigate the surface morphology of as-deposited and annealed coated systems. In addition, the particle induced X-ray emission (PIXE) was

used to get quantitative information of the elemental distribution which in combination with the phase analysis (will be presented in the following part) will provide the information of Pt/Al intermetallics formation.

4.2 Phase analysis by XRD and RBS

The interfacial reactions and phase transformations in the Al-Pt coated systems were studied by X-Ray Diffraction (XRD) and Rutherford backscattering spectroscopy (RBS). The formation of aluminium-platinum intermetallic compounds as a function of annealing (temperature, time) and coating thickness were studied in both coated systems (0.1 μm and 0.3 μm Pt layers deposited on Al substrates). Considering the annealing process, the samples were annealed at different temperatures (from 300 °C to 560 °C) in duration of 30 minutes and an hour. The effects of both annealing temperature and time on the formation of aluminium-platinum intermetallic compounds were investigated. Figure 4.17 shows the XRD spectra of the as-deposited 0.1 μm Pt deposited on Al compared with that annealed at different temperatures for 30 min.

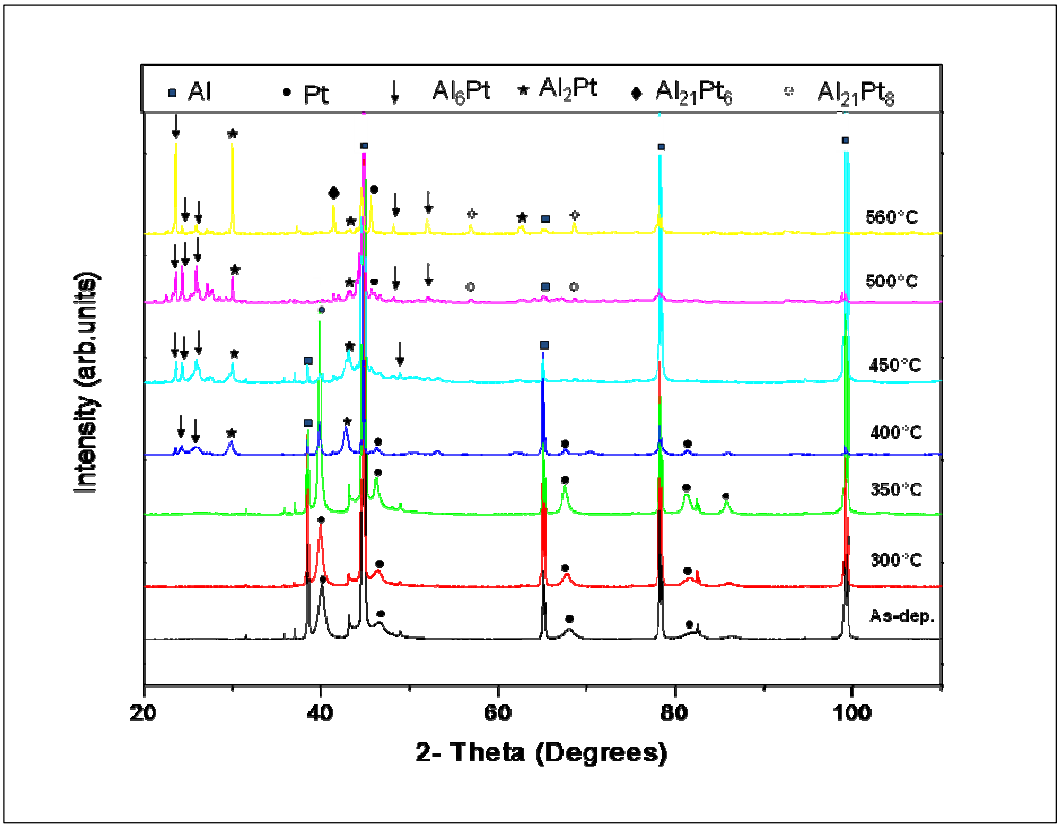

Figure 4.17: X-ray diffraction patterns of 0.1 µm Pt coatings for as-deposited and samples annealed at different temperatures for 30 min.

The phase analysis results show no formation of the Al/Pt intermetallic compounds when the samples were annealed at 300 °C and 350 °C while two phases, Al_2Pt and Al_6Pt, were detected at 400 °C and 450 °C. After annealing at higher temperature (500 °C) the additional phase $Al_{21}Pt_8$ was determined. The XRD spectra obtained for the annealing at 560 °C is similar to the XRD spectrum obtained for 500 °C; formation of new Al/Pt phases have not been detected.

Considering the phase formation of the thin Pt coating (0.1 µm) subjected to annealing, it is evident that all the phases formed at different annealing temperatures are the aluminium rich phases. The limiting element in this system is Pt and the relative concentrations of the reactants was expected to go to the Al rich side after the

Pt has been consumed according to the Walser-Bene and effective heat of formation models **[11, 13]**. The formation of the $Al_{21}Pt_8$ at 500 °C showed that the relative concentration of the reactants has moved to the Al rich side of the effective heat of formation diagram.

However, the results obtained in this study do not correspond fully to the findings of other researchers. Topić *et al.* **[10]** reported the formation of the Al_3Pt_2 phase around 250 °C in nitrogen atmosphere and at 300 °C in air conditions. The annealing environment could be one of possible reasons causing these discrepancies. Namely, thin layer (0.1 μm) of Pt deposited on thick Al substrate (Al>Pt) was studied in this project while the other researchers used the coated system with significantly thicker Pt coating. On other hand, the other researchers Topić *et al.* **[10]** studied thin Pt films deposited on Si wafer. The other possible reason for this discrepancy could be attributed to larger annealing steps (50 °C) used in this study and thus, the formation of particular phase could be missed out.

Besides the phase analysis by XRD the other technique, RBS was also used to study the reactions between Al and Pt. Figure 4.18 shows 2 MeV RBS spectra of the 0.1 μm Pt thick coating subjected to elevated temperatures. The was no interaction of Pt and Al at 350 °C as it can be seen from the RBS spectra that the heights of the Pt signal for the as-deposited and 350 °C samples are the same and there was no shift or change in Pt energy (ΔE_{Pt}) between the two spectra. The Pt layer on the 350 °C annealed sample became a bit thicker (thickening of the coating) than the as-deposited sample during annealing that is the reason why it is not exactly at the same energy position as the as-deposited. The RBS spectra shows a shift of the Pt signal to lower energies and a drop in the Pt signal height when annealed at 400 °C and at higher

temperatures while a change in the Al signal (ΔE_{Al}) was also observed which implies that there were Al-Pt compounds formed. These findings are consistent with the phase analysis results. X-ray diffraction confirmed that there was no compound formation occurred when annealing at 350 °C and temperatures below.

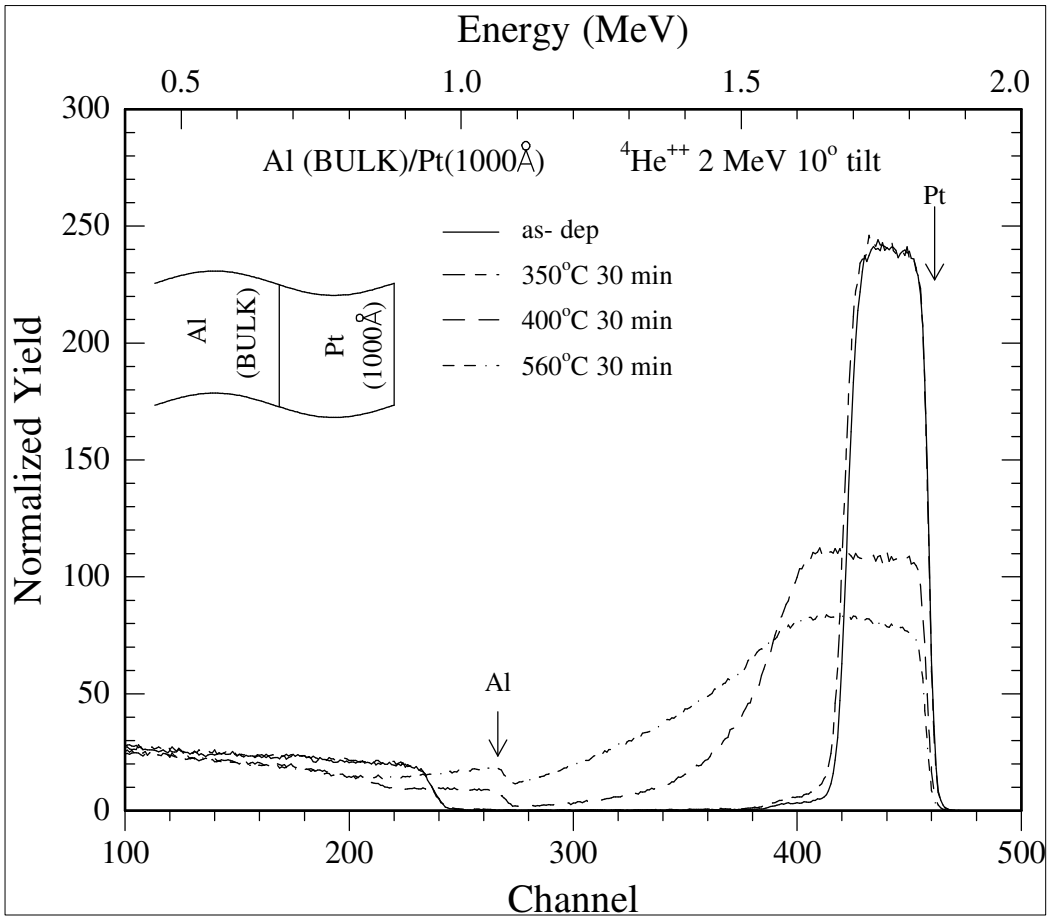

Figure 4.18: RBS spectra of 0.1 µm Pt layer deposited on thick Al substrate: (a) as-deposited, and samples annealed at (b) 350 ºC, (c) 400 ºC, (d) and 560 ºC for 30 min.

Figure 4.19 shows the X-ray diffraction patterns of the as-deposited 0.1 µm Pt layer and that annealed from 350 °C to 500 °C for an hour.

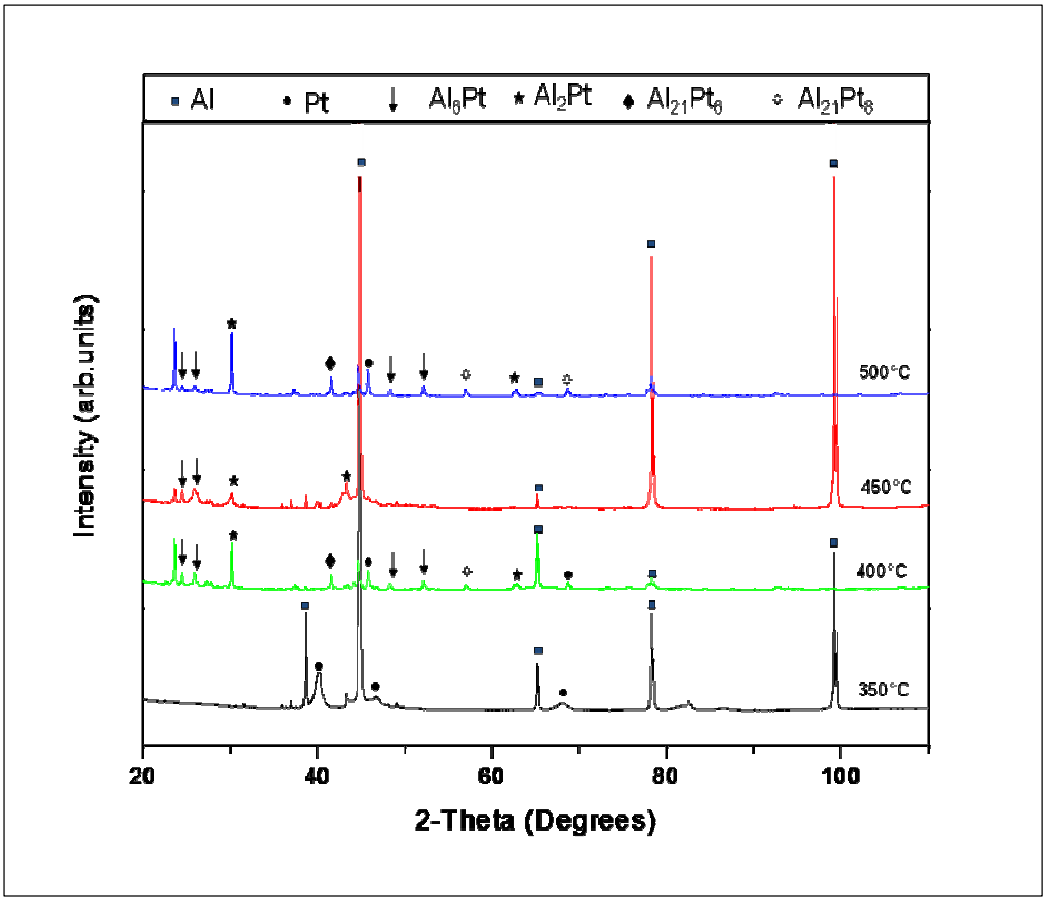

Figure 4.19: X-ray diffraction patterns of 0.1 µm Pt coating. Sample were annealed at 350 ℃, 400 ℃, 450 ℃, and 500 ℃ for a duration of 1 hr.

No compound formation could be observed between Al and Pt at 350 ℃ after annealing for 1 hr. Annealing the sample up to 400 °C for an hour lead to formation of two phases $Al_{21}Pt_8$ and $Al_{21}Pt_6$. However, annealing the sample at 500 °C for 1 hr exhibits the $Al_{21}Pt_6$ phase. These findings shows that the annealing time plays an important role in formation and stability of intermetallics in the Al/Pt coated systems used in this study. However, it should be mentioned that the fitting of data was exceptionally difficult and therefore, the information on phase formation and identification of phases was not possible using this technique.

The XRD experiments were also performed using the samples where thicker Pt layers (0.3 µm) were deposited on Al substrates. Figure 4.20 show the phase analysis results for as-deposited and annealed conditions.

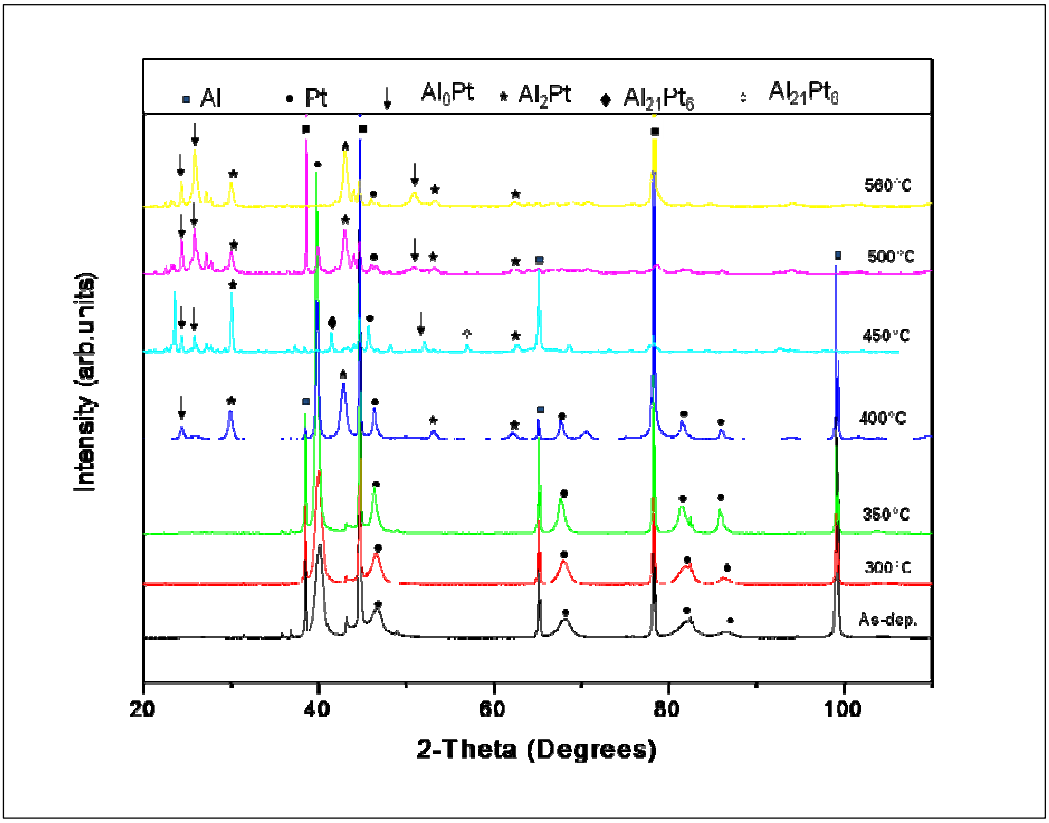

Figure 4.20: X-ray diffraction patterns of 0.3 µm coating annealed at 300 °C, 350 °C, 400 °C, 450 °C, 500 °C and 560 °C for the 30 min.

The findings are similar as for the thin Pt layer (0.1 µm) systems; no new phase formation was detected when the annealing temperature was lower than 350 °C. Diffraction peaks originated from Al-Pt compound reflections were observed at 400 °C and higher temperatures. There was no much difference with the results of the 0.1 µm Pt coating shown in fig. 4.17 except that the $Al_{21}Pt_6$ peak was not observed on the 0.3 µm Pt coatings annealed at 560 °C. Some of the Pt peaks disappeared in the 560 ºC annealed sample; this was an indication that the Pt has been consumed for the

formation of new intermetallic phases. The three intermetallic phases i.e. Al_2Pt, Al_6Pt, and $Al_{21}Pt_8$ were observed for both annealing temperatures, 400 ºC and 560 ºC. RBS results for the 0.3 µm Pt film coating (as-deposited and annealed at 350 ºC, 400 ºC, and 560 ºC for 30 min) are shown in Fig. 4.21.

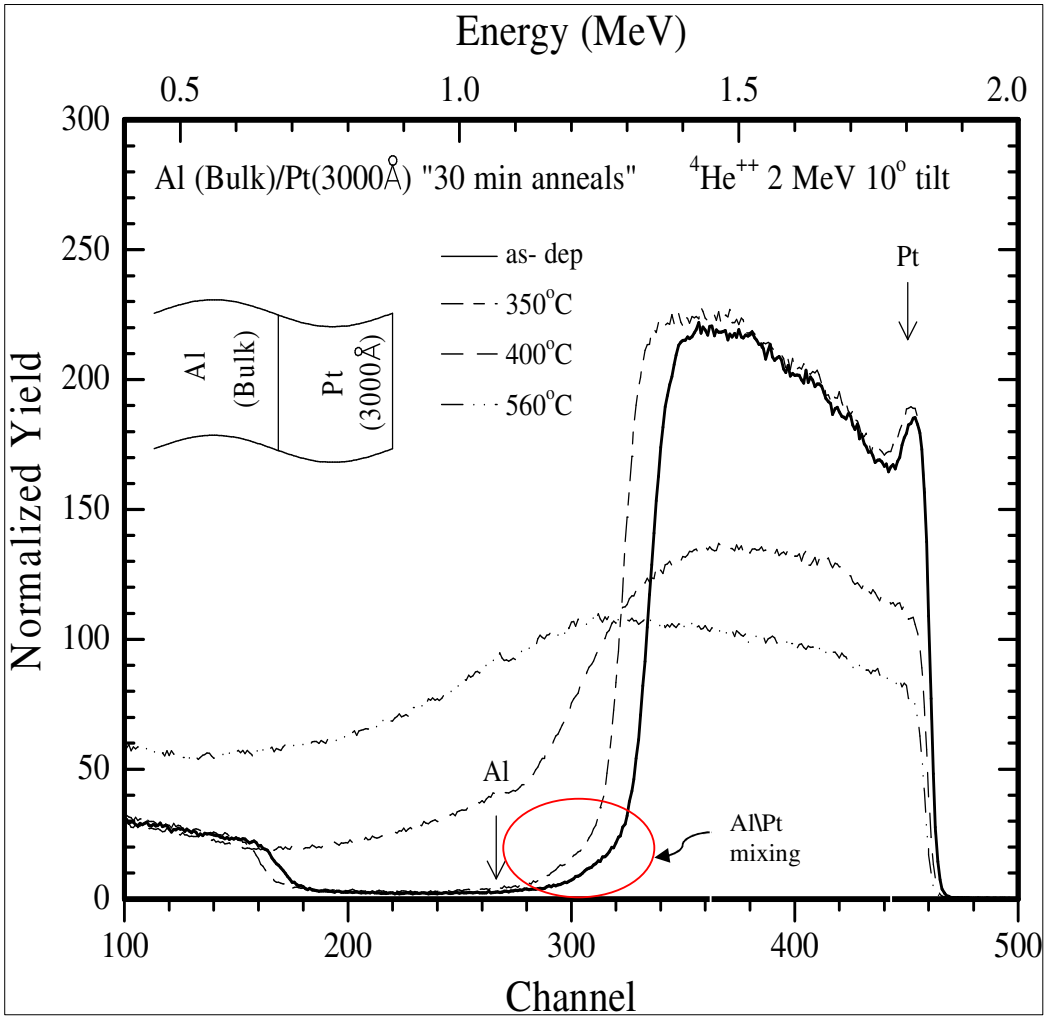

Figure 4.21: Plot of 2 MeV $^4He^{++}$ 10° tilt RBS spectra of the 0.3 µm Pt layer: (a) as-deposited and samples annealed at different temperatures for 30 min.

The spectra show that there was interfacial reaction between Pt and Al in the sample annealed at 350 °C The tails around channel 300-400 indicates the interdiffusion of Pt in the Al. From fig. 4.21 it is clear that the Pt peak width increased after annealing at

350 °C, and that the Al edge moves to lower energies. This is consistent with Al dilution into the Pt layer. Thickening of the coating layer (Pt) as well as interdiffusion between Pt and Al during annealing can be used to explain the discrepancies observed in the as-deposited and 350 °C spectra. Formation of Pt/Al intermetallic compounds was observed when annealing at 400 °C and higher temperatures. The broadening of the Pt signal and reduction of Pt signal height is an indication of new compound formation at 400 °C and 560 °C annealed samples. Similarly as for thin Pt layer of 0.1 μm, no compound formation at 350 °C. A new emerging phase $Al_{21}Pt_8$ by identified by XRD was observed at 450 °C.

Figure 4.22 represents the X-ray diffraction patterns for the 0.3 μm thick Pt layer annealed at temperatures from 350 °C to 500 °C. It has been observed that all the intermetallic phases annealed with Pt/Al systems (Al_2Pt, Al_6Pt, $Al_{21}Pt_8$, and $Al_{21}Pt_6$) were observed in the samples annealed at 400-500 °C for 30 min and 1 hr respectively.

The formation of $Al_{21}Pt_6$ was observed after annealing for an hour at 400 °C, $Al_{21}Pt_6$ phase was not present in the sample annealed for 30 min. The experimental X-ray data collected at room temperature, 300 °C, and 350 °C showed that there were no intermetallic phases formed. It can be speculated that the formation of this phase was missed since big annealing temperature steps of 50 °C was used in this experimental work. Another factor which might have hindered the formation of the intermetallic phases is the short holding time of 30 min and 1 hr.

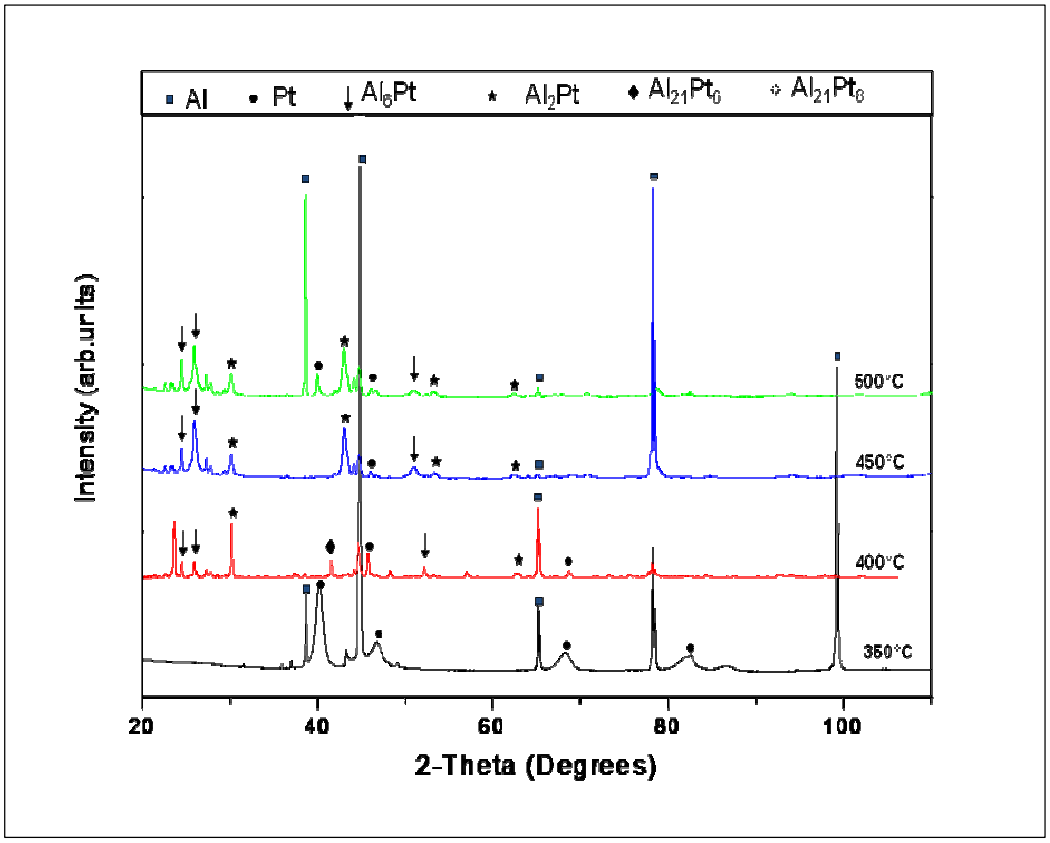

Figure 4.22: X-ray diffraction patterns of the 0.3 µm Pt thick coating annealed at 350 ℃, 400 ℃, 450 ℃, and 500 °C for 1hr.

Finally, the phase formation and the sequence of phase formation have been studied by two techniques: X-ray diffraction (XRD) and the Rutherford backscattering spectrometry (RBS). Both techniques complementary provided useful information about phase transformation in two Al/Pt coated systems. In chapter 5 the intermetallics observed in this study are compared with the phases predicted by the effective heat of formation model.

CHAPTER 5 DISCUSSION

Intermetallics formation in the Pt-Al binary system at temperatures in the range of 200-600 ºC have been investigated by the study of thin platinum coatings (0.1 μm Pt and 0.3 μm Pt layers) deposited on thick aluminium substrates. In order to characterize the changes caused by elevated temperature several techniques such as microscopy, X-ray diffraction and nuclear microprobe techniques were used.

The main focus of this research was placed on the morphology of coated systems and changes caused by annealing treatment. The SEM images (figs. 4.2-4.12) show the morphologies as a function of coating thickness, temperature and annealing time. The morphological studies show that several mechanisms such as roughening, wrinkling, thickening, cracking and delamination have contributed to degradation of annealed coatings.

It has been observed that the surface of Pt coatings significantly change after annealing particularly at higher temperature, although the changes were influenced by thickness of deposited layer. It appeared that the surface morphology of the Pt/Al system with thick Pt layer (0.3 μm) became significantly more uneven and generally more damaged after annealing at higher temperature in comparison to systems with thin platinum layer (0.1 μm). In addition, the presence of "precipitates" has been observed at higher annealing temperatures (e.g. 500 °C and 560 °C) irrespectively of coating thickness. The energy dispersive spectroscopy (EDS) analysis show that these precipitates consist of approximately 64 at.% Al and 36 at.% Pt and it corresponds to the chemical composition of Al_2Pt ($Al_{0.66}Pt_{0.33}$) intermetallic compound. Considering

the annealing time, no significant difference in coating morphology was observed after longer treatment (1 hr and 30 min in this study).

Based on the experimental results obtained in this study, it was established that all factors such as thickness of deposited layer, annealing temperature and time play crucial role determining the morphology of annealed Pt/Al coated systems. The morphological changes have been attributed to formation of several Pt/Al intermetallic phases. On the other hand, the thermodynamics and kinetics of phase transformation in coated systems and ultimate formation of intermetallics depend on many factors. During annealing the atoms of the two reacting species change their original lattice positions through diffusion. When Al and Pt atoms swap positions in an interstitialcy diffusion mechanism or when a Pt atom jumps to an unoccupied Al lattice site that causes strains in the material because the atomic radius of the two materials are different, Pt atomic radius: 1.35 Å and Al atomic radius: 1.25 Å **[28-30]**. The distortion of planes during diffusion as a result of atoms forcing their way to interstitial site can result in an irregular or uneven surface morphology. Although the atomic size factor cannot be avoided but annealing at a specific temperature can bring atoms at the right lattice site positions and the surface of the coating can be improved. In general, the surface morphology of the coating such as roughness can be affected by many factors, including the quality of the substrate, the thermal coefficient mismatch between the substrate and the coating. Pedraza *et al.* **[42]** reported that rumpling or "roughening" is a defect that results not only from the differences between the thermal expansion coefficients but also due to different mechanical properties of coating and the substrate. They found that the coating volume changes during annealing and consequently, rumpling of coatings occurs. This mode of coating damage was also observed by Yin *et al.* **[39]**; they have discovered that the

formation of intermetallic compounds is directly responsible for the volume change. The strain in thin Pt films caused by volume changes during the formation of intermetallics can be relaxed by the growth of the phase/s towards surface areas. However, the strain caused by volume change is complicated to eliminate; the strains due to the volume change from the layer of mixed phases cannot be easily relaxed and thus promote the formation of uneven structures. It can be said that the surface features of the coatings depend on the manner in which intermetallic compounds form (growth mode).

The phase analysis results (Tables 5.1-5.2) show that four Al-rich phases were formed in Pt/Al coated systems investigated in this study: Al_2Pt, Al_6Pt, $Al_{21}Pt_8$, and $Al_{21}Pt_6$. The X-ray diffraction (XRD) of the thin (0.1 μm) Pt coatings (Table 5.1) showed that two phases, Al_2Pt and Al_6Pt, were formed simultaneously at 400 °C and they remained stable until 500 °C and 560 °C. However, annealing treatment at 500 °C and 560 °C promoted formation of additional phases, $Al_{21}Pt_8$ and $Al_{21}Pt_8$, respectively.

Table 5.1: Experimental results of intermetallic compounds formed during annealing of the 0.1 μm Pt coating at elevated temperatures for 30 min.

≤ 350 °C	400 °C	450 °C	500 °C	560 °C
-------	Al_2Pt	Al_2Pt	Al_2Pt	Al_2Pt
-------	Al_6Pt	Al_6Pt	Al_6Pt	Al_6Pt
-------	-------	-------	$Al_{21}Pt_8$	$Al_{21}Pt_8$
-------	-------	-------	--------	$Al_{21}Pt_6$

In the Pt-Al systems with thick Pt layer (0.3 μm), the Al_2Pt and Al_6Pt phases started to be observed at 400˚C. An increase in annealing temperature to 450˚C resulted in the formation of additional two phases ($Al_{21}Pt_8$ and $Al_{21}Pt_6$). However, Al_2Pt and Al_6Pt intermetallic compounds remained stable until high annealing temperature (500 °C and 560 °C), Table 5.2.

Table 5.2: Intermetallic phases formed during heat treatment of the 0.3 μm Pt coating for 30 min.

≤ 350 °C	400 °C	450 °C	500 °C	560 °C
-------	Al_2Pt	Al_2Pt	Al_2Pt	Al_2Pt
-------	Al_6Pt	Al_6Pt	Al_6Pt	Al_6Pt
-------	-------	$Al_{21}Pt_8$	------	------
-------	-------	$Al_{21}Pt_6$	-------	-------

The X-ray diffraction results show that there was no compound formation at 300 ^oC and 350 °C for both 0.1 μm and 0.3 μm Pt coatings. Factors such as big annealing temperature steps, short annealing times and annealing atmosphere are among possible reasons. The effect of annealing atmosphere on intermetallic phase formation was reported by Topić *et al.* **[10].** They reported the formation of Pt_2Al_3 at 250 °C (nitrogen environment) and at 300 °C (air condition). Other researchers including Pretorius *et al.* **[1]** found the Pt-Al intermetallic compounds formed between 250 °C and 350 °C. This inconsistency in comparison with the results obtained in this study might be due to the fact that their investigated thin films deposited on Si-wafer while our research considered relatively thick Pt coatings deposited on thick aluminum substrates.

In addition to XRD technique, Rutherford backscattering spectroscopy (RBS) was employed for phase analysis of annealed coated systems. RBS was used to examine interaction between Al and Pt and to detect the presence of light elements like oxygen since annealing was performed in an unprotected environment. However, it was not possible to identify phases due to difficulties in simulating the spectrum. The difficulty in simulation of RBS was believed to be caused by island formation of intermetallic phase instead of layer by layer formation. This assumption is supported by the SEM and PIXE findings where islands were observed on the coating.

The experimental results obtained in this study show that only Al-rich phases were formed upon annealing. This can be explained using the Walser-Bene and EHF models. The EHF model states: *"After first-phase formation in metal-metal binary systems, the next phase to form at the interface between the compound phase and remaining element is the next phase richer in the unreacted element, which has the most negative effective heat of formation"*. In the systems used in this study, more Al was available compared to Pt and thus, the Pt will be completely consumed before Al. The effective concentration of the Pt was reduced by its consumption during the reaction and this lead to the relative concentration of the reactants to move to the left of the effective heat of formation diagram (see fig. 2.4) which is the Al-rich side. The phase formation predicted by this model has been confirmed by the work by Topić *et al*. **[10]**. Their study of thin aluminium coatings on thick platinum substrates showed that the Pt_2Al_3 intermetallic phase was the first phase formed as predicted by the EHF model. This phase was followed by the formation of intermetallic phases which are on the Pt–rich side of the effective heat of formation diagram (see fig. 2.4). The presence

of more Pt than Al initiated the transformation of Pt_2Al_3 to PtAl and followed by the Pt_3Al intermetallic phase.

According to the EHF model (section 2.4.2) the phase Al_2Pt is expected to form first because it is the one with the most negative EHF value. It has small number of atoms in its unit cell and its formation will lead to the biggest change in free energy. Considering the intermetallic phases observed in both coated systems investigated in this study, there are two stable phases (Al_2Pt and $Al_{21}Pt_8$) as shown in presently available equilibrium phase diagram. The other two intermetallic compounds Al_6Pt and $Al_{21}Pt_6$ are not equilibrium phases and therefore, they are not shown in the Pt-Al phase diagram.

CHAPTER 6 SUMMARY AND CONCLUSIONS

The characterization of Aluminum/Platinum coated systems having different thickness of platinum layers (0.1 μm and 0.3 μm) deposited on thick aluminium substrates and subsequently annealed up to 590 °C have been performed by several complementary techniques. The formation of intermetallic phases has been studied as a function of annealing parameters (temperature and time) and coating thickness. The following conclusions can be draw from this study:

- Annealing temperature effects the coating morphology while the annealing time does not have significant effect on morphology

Generally, the coatings became significantly rougher after annealing at higher temperatures. It was also observed that annealing time has no significant influence on coating morphology. However, both effects were more pronounced in the systems with thick platinum layer. The surface roughening, delamination, cracking and thickening were identified as the major degradation mechanisms in the Al/Pl coated systems investigated in this study. In addition, annealing at temperature close to melting point of aluminium (500 °C and 560 °C) caused formation of "cubical precipitates" in both systems.

- Annealing process promotes phase transformation and formation of intermetallic phases.

Four Al-rich intermetallic compounds have been determined in the Al/Pt coated systems: Al_2Pt, Al_6Pt, $Al_{21}Pt_8$ and $Al_{21}Pt_6$

Thin platinum coating (0.1 μm) - The annealing heat treatment at temperatures up to 350 °C does not affect the formation of Al/Pt intermetallic phases while two phases (Al_2Pt and Al_6Pt) were detected at 400 °C and 450 °C: Additional phase, $Al_{21}Pt_8$, was detected when the system was annealed at 500 °C. Finally, annealing of thin Pt coatings at 560 °C resulted in the formation of four intermetallic phases: Al_2Pt, Al_6Pt, $Al_{21}Pt_8$ and $Al_{21}Pt_6$.

Thick platinum coating (0.3 μm) – The same phases have been detected at 400 °C while annealing at 450 °C caused formation of four phases: Al_2Pt, Al_6Pt, $Al_{21}Pt_8$ and $Al_{21}Pt_6$. However, high temperatures (500 °C and 560 °C) contributed towards instability of some phases resulting that only two phases, Al_2Pt, Al_6Pt, were fund stable at high temperature.

- The changes in coating morphology have been attributed to formation of intermetallic phases.

- The phase analysis results show that the phases determined in the Al/Pt coated systems are not fully in agreement with predictions made by effective heat of formation (EHF) model. It is due to the fact that the experimental methodology included high measuring steps (50 °C) and the formation of some phases has been missed out.

- The results obtained by several complementary techniques serve as a good base for further study of the Pt-Al system. However, to be able to tailor the properties of this coated system for particular applications, the other aspects such as residual stress need to be incorporated into this study.

Recommendations

- Special care should be taken on annealing temperature steps in order not to miss out the temperature in which some of the phases form. Small steps of 10 °C or 20 °C are recommended.

- The use of real-time techniques such as real-time XRD and real-time RBS is strongly recommended in order to follow intermetallic phase formation in the system.

- The thickness of the coating must be carefully chosen because it showed some effects on the morphology of the coating.

- The link between crystallography and morphological changes can also be an interesting topic to look at, and for this reason technique such as the electron backscattered diffraction (EBSD) can be used.

- The study of intermetallic phase formation at different annealing environments must also be taken into consideration.

REFERENCES

[1] A. Kovacs, P.B Barna, Solid State Ionics 141-142 (2001), pp 105-108.

[2] A. Kovaćs, P.B Barna, J.L Lábár, Thin Solid Films 433 (2003), pp 78-81.

[3] C.V Thomson, J. Mater. Res. 7 (1992) 367.

[4] R Pretorius, R de Reus, AM Vredenberg, FW Saris, J. Appl. Phys. 70, (1991) 3636.

[5] E.G.Colgan, C.-Y. Li, and J.W. Mayer, J.Mater.Res.2 (5), (1987), pp 557-566.

[6] T. K. Marais, Phase formation sequence in metal-semiconductor and metal-metal thin films system (1993), Ph.D thesis, University of Western Cape, South Africa.

[7] C. Bergman, P. Gas, D. Mangelinck, Journal of Electroanalytical Chemistry 584 (2005), pp 23-27.

[8] K. Tammeveski, T. Kikas, T. Tenno, L. NiinistÖ, Sensors and Actuators B 47 (1998), pp 21-29.

[9] K. Tammeveski, T. Tenno, J. Ninisto, T. Leitner, G. Friedbacher, and L. Ninisto, Applied Surface Sciences, vol.156, issues 1-4, (2000), pp 135-142.

[10] M Topić, CA Pineda-Vargas, R Bucher, H.E du Plessis, B. Breedt, V. Pischedda, S Nxumalo, C. I Lang, Surface & Coatings Technology 203 (2009), pp 3044-3048.

[11] R.Pretorius, A.M Vredenberg, and F.W. Saris, J. Appl. Physics 70 (7), (1991), pp 3636-3645.

[12] R. Pretorius, C.C Theron, T.K Marais, and H.A. Ras, Mater. Chem. Phys, (1993) 31.

[13] C.C. Theron, O.M. Ndwandwe, J.C. Lombaard, R. Pretorius, Materials Chemistry and Physics 46 (1996), pp 238-247.

[14] F.M d'Heurle, P. Gas, "Kinetics of formation of silicides: A review", J. Mater. Res. 1 (1986), p 205.

[15] M G.I. Vorobets, O.I. Vorobets, and V.N. Strebegev, Applied Surface Science, Vol. 247, Issues 1-4, (2005), pp 590-601.

[16] D. R. Askeland, The Science and Engineering of Materials, (PWS –KENT Publishing Company, Boston, 1985).

[17] C.C Theron, In situ, real-time characterization of solid-state reaction in thin films (1997), Ph.D thesis, University of Stellenbosch, South Africa.

[18] B. Borer, A. Sonnenfeld, and Ph. Rudolf von Rohr, Surface and Coatings Technology, Vol. 201, Isssues 3-4, (2006), pp 1757-1762.

[19] D.A. Porter, and K.E. Easterling, Phase Transformations in Metals and Alloys, (Van Nostrand Reinhold (International) Co.Ltd, 1981).

[20] Jnr. W. D. Callister, Materials Science and Engineering, (John Wiley & Sons, Inc, 2003).

[21] R. Pretorius, T.K. Marais and C.C. Theron, Thin film compound phase sequence, Materials science and engineering, 10 (1993) pp 1-83.

[22] P-F. Yang, S-R. Jian, Y-S. Lai, C-S. Yang, and R-S. Chen, Journal of alloys and compounds 463 (2008), pp 533-538.

[23] O.M Ndwandwe, phase formation sequence at metal-Germanium interfaces in thin film systems (1996), Ph.D thesis, University of Zululand, South Africa.

[24] A.D.L. Humpris, M.J. Miles, and J.K. Hobbs, Applied physics letters 86, 034106 (2005).

[25] L. C.Feldman and J. W.Mayer, Fundamentals of surface and thin film analysis, (Elsevier Science Publishers B.V, 1986), pp 13-66.

[26] P.J Goodhew, J. Humphreys, R. Beanland, Electron Microscopy and Analyses, (Taylor and Francis Group, 2001, pp 122-166.

[27] M.T. Postek, K.S. Howard, A.T. Johnson, K.L. M^{c}Michel, Scanning Electron Microscopy, (Ladd Research Industries, 83 Holly Court, Williston, Vermont, 2001)

[28] R.A. Serway, Physics for scientist and engineers, 2nd edition (Saunders college publishing company, 1986).

[29] W.G. Marburger, C.W. Hoffman, Physics for our times, (McGraw-Hill book company, INC. 1958).

[30] J.B. Marion, W.F. Hornyak, Physics for science and engineering, (CBS College publishing, 1982).

[31] L.W. Taylor, Physics the pioneer science, Vol.2 (Dover publications, Incl. New York, 1959).

[32] F. Lobkowics, A.C. Melissinos, Physics for scientist and engineers, Vol.2 (W.B Saunders company, 1975).

[33] The Rigagu Journal, Vol. 10/ number 1 (1993).

[34] I. M. Govil, Proton induced x-ray emission- A tool for non-destructive trace elements analysis, Current science Vol. 80, (2001), pp 1542-1549.

[35] Z.B. Alfassi, M. Peisach, Elemental analysis by particle accelerators, (CRC PRESS, Boca Raton Ann Arbor London, 1992).

[36] F. Watt and G.W. Grime, Principles and application of high-energy ion microbeams, (Adam Hilger publishers, Bristol, 1987).

[37] W-K. Chu, J.W. Mayer, and M-A. Nicolet, Backscattering Spectroscopy, (ACADEMIC PRESS, New York, 1978).

[38] E.G.Colgan, C.-Y. Li, and J.W. Mayer, Appl. Phys, Vol. 51, No. 6, (1987), pp 424-426.

[39] J. Yin, W. Cai, Y. Zheng, and L. Zhao, Effect of Pt film thickness on the PtSi formation and film surface morphology, Vol. 198, issues 1-3, (2005), pp 329-334.

[40] R. Pannat, S. Zhang, and K.J. Hsia, Acta Materialia 51 , Vol.51, issue 1, (2003), pp 239-249.

[41] M. Wen, E.H Jordan, and M. Gell, Surface and Coating Technology 201 (2006), pp 3289-3298.

[42] F. Pedraza, A.D. Kennedy, J. Kopecek, and P. Morreto, Surface & Coatings Technology, Vol.200, issues 12-13, (2006), pp 4032-4039.

[43] M.C Li, L.C Zhao, X.H Zhen, X.K Chen, Materials Letters 57 (2003), pp 3735-3740

Appendix

Table A: Room – Temperature Linear Coefficient of Thermal Expansion Values for Various Engineering Materials

	Coefficient of Thermal Expansion	
Material	**$10^{-6}(°C)^{-1}$**	**$10^{-6}(°F)^{-1}$**
Ductile irons		
• Grade 60-40-18	11.2	6.2
• Grade 80-55-06	10.6	5.9
Alluminium Alloys		
Commercially pure Al*	23.6	13.1
Alloy 1100	23.6	13.1
Alloy 2024	22.9	12.9
Alloy 6061	23.6	13.1
Alloy 7075	23.4	13.0
Alloy 356.0	21.5	11.9
Magnesium Alloys		
Alloy AZ31B	26.0	14.4
Alloy AZ91D	26.0	14.4
Titanium Alloys		
Commercially pure (ASTM grade 1)	8.6	4.8
Alloy Ti-5Al-2.5Sn	9.4	5.2
Alloy Ti-6Al-4V	8.6	4.8
Precious Metals		
Gold commercially pure	14.2	7.9
Platinum commercially pure*	9.1	5.1
Silver commercially pure	19.1	10.9

Sources: Jnr. W.D Callister, Materials Science and Engineering, (John Wiley & Sons, INC 2003) and Science and Engineering textbook by D.R Askeland (PWS-KENT publishing company, Boston, 1985).

Appendix

Table B: Melting Temperatures of some Common Engineering Materials

	Melting Point	
Material	**(°C)**	**(°F)**
Aluminium*	660	1220
Beryllium	1285	2345
Chromium	1860	3380
Cobalt	1495	2723
Copper	1084	1983
Gold	1063	1945
Iridium	2450	4440
Iron	1536	2797
Lead	327.5	621
Magnesium	650	1200
Manganese	1244	2271
Molybdenum	2620	4750
Nickel	1453	2647
Osmium	3025	5477
Platinum*	1770	3220
Plutonium	640	1180
Potassium	63.3	146
Silicon	1411	2572
Silver	961	1760
Tantalum	2980	5400
Titanium	1670	3040
Tungsten	3400	6150
Uranium	1132	2070
Vanadium	1900	3450
Zinc	419.5	787

Sources: Jnr. W.D Callister, Materials Science and Engineering, (John Wiley & Sons, INC 2003) and Science and Engineering textbook by D.R Askeland (PWS-KENT publishing company, Boston, 1985).

*Materials used in this study.